Oceanologia 64 (2022) 514—534

Available online at www.sciencedirect.com

ScienceDirect

journal homepage: www.journals.elsevier.com/oceanologia

ORIGINAL RESEARCH ARTICLE

A coupled model for sediment transport dynamics and prediction of seabed morphology with application to 1DH/2DH coastal engineering problems

Vasileios Afentoulis[a,*], **Andreas Papadimitriou**[a], **Kostas Belibassakis**[b], **Vasiliki Tsoukala**[a]

[a] *Laboratory of Harbour Works, Department of Water Resources and Environmental Engineering, School of Civil Engineering, National Technical University of Athens, Greece*
[b] *School of Naval Architecture and Marine Engineering, National Technical University of Athens, Athens, Greece*

Received 12 August 2021; accepted 18 March 2022
Available online 4 April 2022

KEYWORDS
Sediment transport;
Coastal dynamics;
Boussinesq Wave Model;
Numerical modeling;
Coastal structures

Abstract Coastline retreat poses a threat to nearshore environment and the assessment of erosion phenomena is required to plan the coastal engineering works. The hydromorphodynamic response of a beach to natural and artificial forcing factors differ considerably, as the nearshore processes are especially complex and depended on a multitude of parameters, including prevailing wave and hydrodynamic conditions, beach topography, sediment characteristics and the presence of coastal protection works. The present study serves the purpose of numerically evaluating nearshore morphological processes and ultimately assessing the capacity of coastal defence structures to control beach erosion. For this reason, a new sediment transport model including unsteady effects and swash zone morphodynamics, was coupled to the highly nonlinear Boussinesq wave model FUNWAVE-TVD, providing integrated predictions of bed level evolution, across various timescales of interest. The compound model was vali-

* Corresponding author at: Laboratory of Harbour Works, Department of Water Resources and Environmental Engineering, School of Civil Engineering, National Technical University of Athens, Greece. Tel.: 0033 (0)767943773.
E-mail address: af.vasilis@gmail.com (V. Afentoulis).
Peer review under the responsibility of the Institute of Oceanology of the Polish Academy of Sciences.

Production and hosting by Elsevier

https://doi.org/10.1016/j.oceano.2022.03.007

dated thoroughly against laboratory data and other numerical investigations. Overall, a good agreement between experimental and numerical results was achieved for a number of test cases, investigating the effects of different types of shore protection structures. The proposed integrated model can be a valuable tool for engineers and scientists desiring to obtain accurate bed level predictions, over complex mildly and steeply sloping sea bottoms composed of non-cohesive sediment particles.

List of parameters

Parameter	Description, units
A	Wave amplitude, m
C_d	Bottom friction coefficient
c	Sediment concentration by mass or volume, m^3/m^3
c_a	Reference sediment concentration, m^3/m^3
c_x, c_y	Wave propagation velocities, m/s
d	Diameter of bed material, mm
d_{50}	Median size of sediment, mm
D	Volumetric deposition rate, m^3/s
D_*	Dimensionless particle size
E	Volumetric erosion rate, m^3/s
f_c	Current friction coefficient
f_w	Wave friction coefficient
g	Gravitational acceleration, m/s^2
h	Water depth, m
H	Wave height, m
H_S	Significant wave height, m
H_{m0}	spectral significant wave height, m
K_c, K_l	Cross-shore and long-shore swash coefficients
M	Horizontal flux term
n_p	Sand porosity
k_s	Roughness height, m
q	volumetric net transport rate, m^2/s
R^b	Eddy-viscosity-type breaking term
R^s	Subgrid turbulent mixing term
R	Bottom friction term
Re_*	Shear Reynolds number
T	Wave period, s
T_p,	Peak wave period, s
u	Instantaneous velocity in x direction, m/s
$\bar{u}$	Mean horizontal velocity in x direction, m/s
u_w	Oscillatory horizontal velocity, m/s
$U_{\delta w}$	Near-bottom wave velocity, m/s
u_a	horizontal velocity at adaptive reference level, m/s
U_C	Mean current velocity, m/s
u_*	Shear velocity, m/s^2
u_o	Scaling velocity, m/s
v	Velocity in y direction, m/s
v_o	Scaling velocity in y direction, m/s
w_s	Settling velocity, m/s
z	Vertical distance above the bottom, m
z_a	Reference height, m
β	Parameter of sediment diffusivity
ε	Empirical sediment coefficient
ε_s	Sediment diffusivity, m^2/s
$\varepsilon_{s,c}$	Current-related sediment diffusivity coefficient, m^2/s
$\varepsilon_{s,w}$	Wave-related sediment diffusivity coefficient, m^2/s
Δ_r	Ripple height
δ_w	Thickness of near-bed sediment mixing layer, m
ζ	Water level, m
η	Surface elevation, m
κ	Karman number
θ	Shields number
θ_c	Critical Shields number
ρ	Water density, kg/m^3
ρ_s	Sediment density, kg/m^3
τ	Shear stress, N/m^2
τ_c	Dimensionless critical shear stress
ν_t	Eddy viscosity, m^2/s
ω	Wave frequency, Hz
μ	Dimensionless measure of dispersion
φ_m	Internal friction angle, deg

1. Introduction

Sandy coasts have been constantly modified as a result of natural processes involving wind waves or swell, currents, sea level variability and aeolian sediment transport (Divinsky et al., 2021; Divinsky and Kosyan, 2020; Roelvink and Costas, 2019). Erosion of the coastal seabed and ultimately a retreat of shoreline position is caused by a combination of the abovementioned processes and has strong implications to the economy, environment and community safety since a multitude of activities are concentrated at the coastal zones. Additionally, anthropogenic unplanned infrastructures in the coastal zone, along with jetties and other obstacles to longshore transport, reflective vertical walls that accelerate offshore sand bar migration (Seabergh and Kraus, 2003), as well as devegetation along

coasts are key causes intensifying beach erosion in the long term (Ruiz-Martínez et al., 2016).

The most widely applied engineering technique to control beach erosion is the construction of coastal defense structures, which can also provide sufficient protection against flooding phenomena to the inland (Charlier and De Meyer, 1989; Nordstrom, 2014; Pranzini et al., 2015; Servold et al., 2017; van Rijn, 2013). A variety of coastal defenses can be encountered in the literature of coastal engineering, such as detached emerged and submerged breakwaters, groynes, seawalls, riprap and wave attenuators. Emerged breakwaters, the presence of which leads to reduced wave agitation alters the patterns of the nearshore breaking wave-induced current field and creates the appropriate conditions for sediment deposition, thus enabling shoreline advance. It should be noted that emerged breakwaters have been used at a lesser extent in the recent decades as a protection solution, due to their negative impact on the aesthetic characteristics of coastal landscape. Hence, submerged structures provide a good compromise between the need to reduce the wave energy close to the shore and the aim to ensure landscape preservation and a good water quality though the exchange of water between offshore and inshore areas. Moreover, in case the longshore sediment transport dominates the sediment transport regime, groynes are employed to retain the beach and maintain the stability of the littoral system.

The investigation of nearshore hydrodynamic and morphodynamic patterns, associated with the presence of coastal structures, has been carried out through laboratory experiments during the last decades. In the studies of Ming and Chiew (2000) and Birben et al. (2007) a series of experiments were used to analyze the effect of offshore breakwaters on beach morphology and sediment accumulation ratio. Cáceres et al. (2008) carried out an experimental research to assess wave overtopping and wave-induced current field in the breaker zone around low-crested structures. A new dimensionless parameter (β) was proposed by Mahmoudof and Hajivalie (2021), through experimental investigations in order to describe wave transmission and reflection phenomena over submerged breakwaters. However, scaling effects inherently linked to the experimental conditions and the sediment transport processes (Gorrick and Rodríguez, 2014) render the long-term prediction of coastal bed evolution through experimental procedures a difficult task. As a consequence, process-based models that can advance understanding of the dominant process response (and feedbacks) of littoral systems to a wide range of coastal defense structures, have been extensively used in coastal engineering (Afentoulis et al., 2017; Kobayashi, 2016; Lesser et al., 2004; Nam et al., 2011; Postacchini et al., 2016; Tang et al., 2017; Zyserman and Johnson, 2002).

These composite nearshore models are usually comprised of wave propagation, hydrodynamic, and sediment transport/morphology models. A variety of sophisticated numerical tools have been utilized for the simulation of wave transformation processes, taking into consideration that for most coastal configurations waves are the dominant driving factor, inducing morphological changes. Two distinct approaches have been highlighted (Hotlhiujsen, 2003) for the numerical investigation of the dominant processes governing wave transformation:

1) The phase-averaged approach that describes wave propagation in the spatial and time domain using the variance-density spectrum, which is the Fourier transformation of the auto-covariance function of free-surface elevation. The most notoriously used models following this approach are 3rd generation spectral wave models (Benoit et al., 1997).
2) The phase resolving deterministic approach describing details of the wave field in the spatial and temporal domain at a resolution that is a small fraction of the wavelength / period. In this category, models solving the mild slope, shallow water (SWE), or Boussinesq equations have been employed.

It should be noted that despite the plethora of modeling tools available, each one is associated with flaws, which have to be taken into serious consideration for the purpose of predicting the morphological evolution of coastal areas. Models based on the phase averaging approach are computationally efficient but omit a large number of dominant wave processes in the nearshore, especially considering that wave diffraction, reflection and run-up are not usually accounted for. In addition, coherencies observed in the wave field and caused by abrupt bottom variations and strong current gradients are unable to be simulated in these models (Smit et al., 2015). Phase resolving models are able to resolve many of the aforementioned important wave transformation processes but are often associated with major constraints, i.e. mildly sloping bottoms (for models based on the mild slope wave equations) and satisfaction of the shallow water approximation (for the SWE wave models). From deep to shallow water, dispersive nonlinear wave effects can be simulated satisfactorily using Boussinesq models (Kennedy et al., 2001; Madsen et al., 1997) since they are sufficiently accurate in resolving nearshore wave phenomena, such as refraction and diffraction (Do et al., 2020). However, until recent decades, their application to hydrodynamic modeling in engineering projects was limited due to high computational cost (Klonaris et al., 2018, 2020) rendering their use in practical applications almost impossible.

Nowadays, several Boussinesq-type models coupled with a sediment transport module, suitable for coastal engineering applications, can be encountered in the literature of coastal engineering (Gallerano et al. 2016; Karambas and Koutitas, 2002; Karambas, 2012; Klonaris et al., 2016; Kobayashi et al., 2000; Malej et al., 2019). Moreover, different researches have successfully predicted the shoreline evolution and beach morphology in the vicinity of detached breakwaters, groynes, or vertical quay walls (Bouvier et al., 2019; Ding and Wang, 2008; Hieu et al., 2020; Karambas and Samaras, 2017). Tsiaras et al. (2020) used a nonlinear breaking wave and morphodynamic model, including unsteady aspects of the sand transport for evaluating the potential influence of the transmission coefficient and of the net mass influx over structure in the design process of submerged breakwaters. Moreover, Klonaris et al. (2020) provided a detailed experimental and numerical investigation about the effects of rubble-mound submerged breakwaters on beach morphology, using a compound Boussinesq-type model. Although up to present, numerical predictions of wave-current interactions and morphological responses, with and without the presence of coastal structures, are

still associated with considerable uncertainty related to the highly non-linear nature of these physical processes. In the above-mentioned studies, either the wave and hydrodynamic module does not consider the reflection and transmission (e.g. permeability) characteristics of emerged breakwaters and vertical obstacles, or the utilized sediment transport approximations are not suitable to capture the wave non-linear effects on sand transport and simulate the 3D characteristics of the suspended sediment transport loads.

In the present study, a fully nonlinear Boussinesq model (Shi et al., 2012), FUNWAVE — Total Variation Diminishing (TVD), tasked with the simulation of wave propagation and hydrodynamic circulation was directly coupled to a quasi-3-D sediment transport and morphology model, which was developed by the authors of this study. Thus, taking advantage of FUNWAVE model's capacity to provide information on coastal structure's reflection and transmission behavior and employing advanced sediment transport approximations, including unsteady sand transport aspects, this study seeks to reduce the uncertainty in hydro-morphodynamic predictions. Special attention was given to the role of sediment transport dynamics across the swash zone, incorporating them in the morphodynamic model, while advanced techniques were utilized to model the three-dimensional patterns of suspended load fluxes and consider wave nonlinear and unsteady effects on bed load transport rates. Our scope is to introduce an integrated model that can be utilized to a wide range of maritime engineering applications, both for soft engineering (beach replenishment, sand dune management, drainage) and hard engineering techniques (design of groynes, breakwaters, seawalls, revetments). A particular effort was made to keep the computational complexity at a reasonable level by utilizing morphological acceleration techniques and exploiting the efficient parallel scheme of the wave model. Moreover, in order to ensure the reliability of our numerical modelling approach, the compound model was extensively validated for five distinctive test cases, covering a wide range of coastal engineering applications in both experimental and field scales and providing significant insights into the morphological response of sandy beaches to the combined action of waves and currents.

2. Description of models and formulations

A fully coupled method for simulation of wave-current-seabed interaction was developed within the context of our research. The numerical output of FUNWAVE-TVD model is used as forcing for a two-dimensional sediment transport model in an interactive mode, while the computation of sediment fluxes and morphological changes provides the feedback of bathymetry updates on wave computations. Particularly, the seabed morphology is updated over a morphological time step (Δt_{mor}) and for every bed level update, simulations by three numerical tools are performed: FUNWAVE-TVD model, followed by a sediment transport model and a bathymetry updating module. This process is repeated until a preset duration, coinciding with the simulation end time is reached. The relevant flow chart outlining the model interaction and feedback is illustrated in Figure 1. The implementation of a morphological acceleration factor (Morfac) serves to multiply bed level changes by a nonunity integer quantity and therefore alters the morphology time scale. In this research, three different time scales and steps were utilized in order to simulate nearshore processes of a different nature, the time step (Δt) of the wave model (FUNWAVE-TVD), the time interval of wave action which is necessary to obtain the time averaged (mean) velocities that are referred here as currents (Δt_{cur}) and the morphological time step (Δt_{mor}) which is required to calculate bathymetry updates.

2.1. Hydrodynamics

Wave propagation and hydrodynamic circulation can be simulated by FUNWAVE-TVD model from deep to shallow water, including the surf and swash zone. The governing equations of the above model were based on the fully nonlinear Boussinesq equations (Nwogu et al., 1992), modified by Chen et al. (2003) and Chen (2006) and extended to incorporate a moving reference level (Kennedy et al., 2001). FUNWAVE-TVD is a nonlinear wave model that operates with a hybrid finite-volume and finite-difference TVD-type scheme developed by Shi et al. (2012). The shock-capturing wave-breaking scheme, chosen for this study, was based on the work of Tonelli and Petti (2009). This method takes advantage of the shock-capturing ability of non-linear shallow water equations (NSWE) and can simulate the moving hydraulic jumps. Following the Courant-Friedrichs-Lewy (CFL) criterion, an adaptive time step was implemented, based on a third-order Runge-Kutta scheme for nonlinear spatial discretization. The model includes wetting-drying moving boundary conditions with the incorporation of Harten-Lax-van Leer (HLL) construction method into the scheme. The sponge layer technique introduced by Larsen and Dancy (1983) is used by FUNWAVE-TVD model to deal with internal wave reflection problems. The governing equations of the wave model are presented below:

$$\eta_t + \nabla \cdot \boldsymbol{M} = 0, \tag{1}$$

$$\boldsymbol{u}_{a,t} + (\boldsymbol{u}_a \cdot \nabla)u_a + g\nabla\eta + \boldsymbol{V}_1 + \boldsymbol{V}_2 + \boldsymbol{V}_3 + \boldsymbol{R} + \boldsymbol{R}^b + \boldsymbol{R}^s = 0. \tag{2}$$

Equation (1) represents the depth-integrated mass conservation, while Equation (2) denotes the depth-averaged horizontal momentum. The symbol $\boldsymbol{M}$ of Equation (1) is the horizontal flux and can be further expressed as:

$$\boldsymbol{M} = (h+\eta)\left[\boldsymbol{u}_a + \mu^2\left\{\left(\frac{{z_a}^2}{2} - \frac{1}{6}\left(h^2 - \eta h + \eta^2\right)\right)\nabla(\nabla\cdot\boldsymbol{u}_a)\right) + \right.$$
$$\left. + \left(z_a + \frac{1}{2}(h-\eta)\right)\nabla(\nabla\cdot(h\boldsymbol{u}_a))\right\}\Bigg], \tag{3}$$

where η is the sea-surface elevation, h is the water depth, $\boldsymbol{u}_a$ the horizontal velocity at the adaptive reference elevation, z_a and μ denotes a dimensionless measure of dispersion. In addition, $\boldsymbol{V}_1$ and $\boldsymbol{V}_2$ are the dispersive Boussinesq terms, $\boldsymbol{V}_3$ accounts for the second-order effect of vertical vorticity, $\boldsymbol{R}$ represents the quadratic form of the bottom friction modeled by $C_d\boldsymbol{u}_a|\boldsymbol{u}_a|$, where C_d is the bottom friction coefficient. The term $\boldsymbol{R}^b$ in Equation (2) can be used optionally, to model the eddy-viscosity-type breaking terms

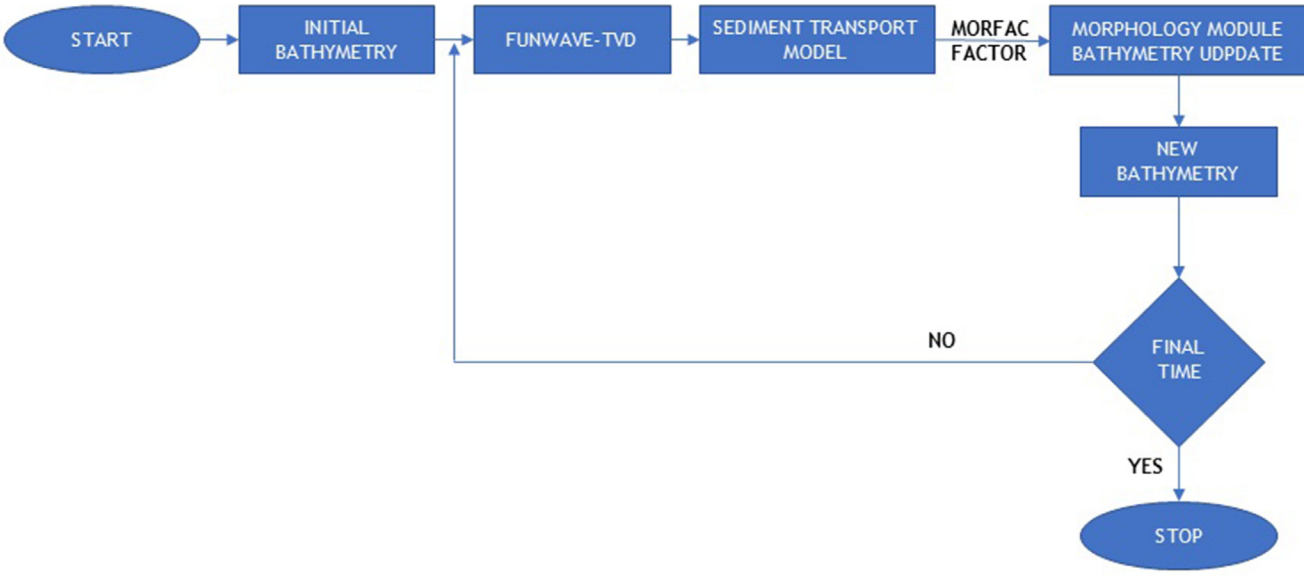

Figure 1 Flow chart of wave-current, sediment transport and morphology models.

(in this study the shock-capturing scheme of Tonelli and Petti (2009) was activated), while the term $\boldsymbol{R}^s$ accounts for the subgrid turbulent mixing (Chen et al., 2003). A Smagorinsky-type (1963) subgrid turbulent mixing algorithm is employed and the eddy viscosity associated with the subgrid mixing is determined by breaking-induced current field (Chen et al., 1999).

FUNWAVE-TVD model can simulate wave-generated nearshore currents, such as rip current or alongshore currents, and eddies due to shear instabilities, estimated via the $\boldsymbol{R}$, $\boldsymbol{R}^b$, $\boldsymbol{R}^s$ dissipative and diffusive terms. In recent studies, Boussinesq models have been utilized to model rip currents (Geiman et al., 2011; Johnson and Pattiaratchi, 2006) and alongshore currents (Chen et al., 2003; Feddersen et al., 2011) in the nearshore zone. Geiman et al. (2011) presented a numerical study on wave averaging effects on estimates of the surf zone mixing. Their study revealed that FUNWAVE-TVD model is able to reproduce 1-h time-averaged mean Eulerian velocities consistent with field measurements and numerical findings.

2.2. Morphodynamics

In the present study, a new numerical model developed by the authors of this paper was applied to assess nearshore morphodynamics. The mode of suspended sediment movement is investigated using Van Rijn's (1993) formula, while a formula for unsteady oscillatory flows, suggested by Ribberink (1998) for the estimation of bed load transport, was implemented. The usage of Van Rijn's approximation serves to distinguish suspended load transport that is computed above a reference height α and bed-load transport, which was estimated using the near-bottom hydrodynamic parameters. It is also suited to assess sediment transport rates in combined breaking or non-breaking wave and current conditions. In the following subsections, the governing equations will be presented. Moreover, it has to be mentioned that the Boussinesq-type 2DH model provided depth-averaged hydrodynamic parameters, that were exploited to extract near-bed flow characteristics and nonlinear time-varying near-bottom wave velocities using the parameterization suggested by Karambas and Samaras (2017), initially proposed by Isobe and Horikawa (1982) and modified by Grasmeijer (2002). This technique is based on the energy flux method, in which the fifth-order Stokes and the third-order cnoidal wave theories were implemented appropriately, according to the applicable range. Two parameters were utilized by Isobe and Horikawa (1982) to represent the asymmetry of the velocity profile, based on laboratory and field experimental results. Thus, wave properties such as the wave profile and water particle velocities can be extracted at an arbitrary depth, based on the offshore wave height and period, local water depth and bed slope without explicitly quantifying skewness. Grasmeijer (2002) modified this approximation to calculate time-varying near-bed orbital velocities using local wave characteristics.

2.2.1. Suspended load transport

Van Rijn (1993) suggested a multi-layer model, describing the time-averaged sediment concentration profile. This profile can be obtained by the integration of the time-averaged convection-diffusion under equilibrium (stationary) conditions. The three-dimensional convection-diffusion (mass-balance) equation for the suspended sediment can be written, as follows:

$$\frac{\partial(c)}{\partial t}+\frac{\partial(uc)}{\partial x}+\frac{\partial(vc)}{\partial y}+\frac{\partial[(w-w_s)c]}{\partial z}-\frac{\partial}{\partial x}\left[\varepsilon_{s,x}\frac{\partial(c)}{\partial x}\right]-\frac{\partial}{\partial y}\left[\varepsilon_{s,y}\frac{\partial(c)}{\partial y}\right]-\frac{\partial}{\partial z}\left[\varepsilon_{s,z}\frac{\partial(c)}{\partial z}\right]=0, \quad (4)$$

in which (u,v,w) = local flow velocities, $(\varepsilon_{s,x}, \varepsilon_{s,y}, \varepsilon_{s,z})$ = local turbulent sediment mixing, w_s = particle fall velocity, and c = sediment concentration.

Integration of Equation (4) with respect to z leads to:

$$\frac{\partial(c_{ave})h}{\partial t}+\frac{\partial(Uc_{ave})h}{\partial x}+\frac{\partial(Vc_{ave})h}{\partial y}-\frac{\partial}{\partial x}\left[\varepsilon_{s,x}h\frac{\partial(c_{ave})}{\partial x}\right]-\frac{\partial}{\partial y}\left[\varepsilon_{s,y}h\frac{\partial(c_{ave})}{\partial y}\right]=S, \quad (5)$$

where c_{ave} is the depth-averaged concentration and (U, V, W) the depth-averaged velocities, and S represents the source term of the convection-diffusion equation that is based on the mismatch between a current and an equilibrium concentration (Galappatti and Vreugdenhil, 1985; Galappatti, 1983). In order to estimate the equilibrium concentration, we need to prescribe the boundary conditions of the problem. Considering that the concentration presents variability in a time-scale much larger than the representative wave period stationary conditions in the surface and in the bed boundary are assumed. Thus, the longitudinal diffusion terms can be neglected in relation to the vertical diffusion term, whilst the unsteady concentration term $(\partial(c_{ave})/\partial t)$ is relatively small with respect to the other terms. Moreover, at the water surface, the vertical diffusive flux through the free surface is equal to zero:

$$-w_s c - \varepsilon_{s,cw}\frac{dc}{dz} = 0, \text{ at } z = \eta. \tag{6}$$

At bed-boundary surface, the vertical mixing or the exchange of sediment fluxes, according to Galappati (1983), can be described as:

$$-w_s c - \varepsilon_{s,cw}\frac{dc}{dz} = D - E, \text{ at } z = z_b, \tag{7}$$

where D is the sediment deposition rate and E being the sediment erosion rate.

The sediment erosion rate was evaluated explicitly, while the deposition rate was included in the transport equation implicitly (Lesser et al., 2004), as follows:

$$\text{Erosion rate}: c_\alpha \frac{\varepsilon_s}{\Delta z}, \text{ Deposition rate}: c_k\left(\frac{\varepsilon_s}{\Delta z} + w_s\right), \tag{10}$$

in which, c_α = sediment concentration at the reference level α, ε_s = sediment vertical diffusion coefficient, Δz = vertical distance from the reference level α to the center of reference cell, and c_k = sediment concentration in the reference cell. The vertical distribution coefficient due to currents can be calculated using a parabolic approximation as proposed by Van Rijn (1993).

Erosion and deposition rates are responsible for the vertical readjustment of the concentration distribution and they were used, herein, in order to estimate sediment source and sink terms throughout the vertical. It should be noted that source and sink terms are not normally time-invariant over depth. However, in this study, we consider the existence of an equilibrium concentration profile, which is adjusted to current conditions within a specific time interval. The adjustment of the depth-averaged concentration to its equilibrium value, for specific time and space scales, was described by Katopodi and Ribberink (1992).

For oscillatory flows, the concentration at the reference level α is expressed as:

$$c_a = 0.015\rho_s \frac{D_{50}}{\alpha}\frac{\left(\frac{\theta-\theta_{cr}}{\theta_{cr}}\right)^{1.5}}{D_*^{0.3}}, \tag{8}$$

where ρ_s = sediment density, α = reference level, D_{50} = median particle diameter of bed material, θ = Shields parameter, θ_{cr} = critical Shields parameter, D_* = non-dimensional particle diameter. The reference level (α) herein, was considered equal to $0.5*\Delta_r$ (wave-induced ripple height), while its maximum value cannot be greater than the 20% of the water column.

The vertical distribution coefficient due to the total wave and current mixing was calculated following Lesser et al. (2004) and Van Rijn (1993). This method provides detailed information of distribution coefficient variations over the water depth and leads to similar turbulent mixing values to those generated by the standard algebraic turbulence (Lesser et al., 2004).

Thus, the vertical distribution coefficient due to currents can be calculated as:

$$\varepsilon_{s,c} = k\beta u_{*,c} z\left(1 - \frac{z}{h}\right) \text{for } z < 0.5h,$$
$$\varepsilon_{s,c} = 0.25k\beta u_{*,c} z(1 - z/h) \text{ for } z \geq 0.5h, \tag{9}$$

where, $\varepsilon_{s,c}$ = vertical diffusion coefficient due to currents, k = von Kármán constant (0.4), $u_{*,c}$ = current related bed shear velocity, β van Rijn's factor (used to describe the difference between fluid and granular diffusion).

The vertical distribution coefficient due to waves is calculated as:

$$\varepsilon_{s,w} = \varepsilon_{s,bed} = 0.004 D_* \delta_s U_{\delta w}, \text{ for } z \leq \delta_s,$$
$$\varepsilon_{s,w} = \varepsilon_{s,max} = 0.035 h H_s / T_P, \text{ for } z \geq 0.5h,$$
$$\varepsilon_{s,w} = \varepsilon_{s,bed} + (\varepsilon_{s,max} - \varepsilon_{s,bed})\left(\frac{z - \delta_s}{0.5h - \delta_s}\right), \text{ for } \delta_s < z < 0.5h, \tag{10}$$

where $\varepsilon_{s,w}$ = vertical distribution coefficient due to waves, δ_s = thickness of the near-bed sediment mixing layer, which was equal to three times the ripple height ($\delta_s = 3 * \Delta_r$), $U_{\delta w}$ = near-bottom wave velocity, D_* = non-dimensional particle diameter. The total vertical diffusion coefficient can be expressed as:

$$\varepsilon_{s,Tot} = \sqrt{{\varepsilon_{s,w}}^2 + {\varepsilon_{s,c}}^2}. \tag{11}$$

Ultimately, after integration of the convection diffusion equation over the time the net suspended sediment fluxes can be expresses as follows:

$$\boldsymbol{q_s} = \left(\overline{c_{ave} h U_c - \varepsilon_{s,x} h \frac{\partial c_{ave}}{\partial x}}, \overline{c_{ave} h V_c - \varepsilon_{s,y} h \frac{\partial c_{ave}}{\partial y}}\right), \tag{12}$$

where, U_c and V_c mean over the depth current velocities.

2.2.2. Bed-load transport

Following the approach suggested by Ribberink (1998), bed-load sediment transport can be calculated using a formula for unsteady oscillatory flows where the instantaneous solid flux is assumed to be proportional to a function of the difference between the actual time-dependent bed shear stress and the critical bed shear stress (Figure 4). Therefore, the nonlinear effects of wave asymmetry on bedload transport rates can be satisfactory predicted using the proposed approach. Ribberink's (1998) formulation has been calibrated towards several flume data sets including wave-current interaction in a plane regime (suspended load negligible) and field data (unidirectional flows in rivers). In total, more than 75 bed-load transport measurements in oscillating water tunnels were utilized to corroborate the validity of this approach (Ribberink, 1998). The solid fluxes can be calculated, as follows:

$$\boldsymbol{q_{SB}} = m_{Rib}\sqrt{(s-1)gd^3}\langle\left(\left|\overrightarrow{\theta(t)}\right| - \theta_{cr}\right)^{n_{Rib}} \frac{\overrightarrow{\theta(t)}}{|\theta(t)|}\rangle, \tag{13}$$

where, $\overrightarrow{\theta(t)} = 0.5 f_{cw}|u(t)|\overrightarrow{u(t)}/[(s-1)gd]$ is the time-dependent Shields parameter with the instantaneous velocity $\overrightarrow{u(t)} = \overrightarrow{U_c} + \overrightarrow{u_w(t)}$, s is the relative density of sediment and f_{cw} the wave-current friction factor. $\langle\ \rangle$: Time-averaged over wave period, and $m_{Rib} = 11$, $n_{Rib} = 1.65$: adjusted coefficients.

2.2.3. Swash zone

The swash zone is the area of the coastal environment where the waves run up and down, dissipating or reflecting their energy after moving towards the shore. The sediment fluxes are often large close to the shoreline because of swash uprush and backwash phases. Sediment transport generated from bed evolution at a swash time scale can be several orders of magnitude larger than those derived from the most of available sediment transport formulas, applied in the surf zone. Thus, numerical models often underestimate this sediment migration and tend to yield sediment transport that decreases too rapidly from the swash zone towards the offshore (Klonaris, 2016; Masselink et al., 2009; Nam et al., 2009). For the estimation of longshore and cross-shore sediment transport in the swash zone, the approximation proposed by Larson and Wamsley (2007) has been used. The net transport rates can be expressed as follows:

$$q_{tc,net} = K_c \frac{\tan\varphi_m}{\tan^2\varphi_m - \left(\frac{dh}{dx}\right)^2} \frac{u_0^3}{g}\left(\frac{dh}{dx} - \tan\beta_e\right)\frac{t_0}{T}, \tag{14}$$

$$q_{tl,net} = K_l \frac{\tan\varphi_m}{\tan^2\varphi_m - \left(\frac{dh}{dx}\right)^2} \frac{u_0^2 v_0}{g}\frac{t_0}{T}, \tag{15}$$

where K_c, K_l are cross-shore and long-shore empirical coefficients, respectively, φ_m is the internal friction angle ($\approx 30°$). v_0, u_0 and t_0 are scaling velocities and time, T is the swash duration (considered equal to the incidence wave period), $\tan\beta_e$ is the foreshore equilibrium slope. The calculation of scale velocities was based on the ballistic theory, while the wave front velocities at the still-water shoreline obtained by FUNWAVE-TVD model were used as initial conditions, for more details see Larson et al. (2004). Equation (15) implies that the cross-shore sediment transport rate is zero if foreshore slope is in equilibrium, while longshore transport still occurs if the transporting velocity v_0 is not zero during the uprush and backwash phase. In order to define the foreshore equilibrium, slope the methodology suggested by Larson and Wamsley (2007) and Larson et al. (2004) was applied herein. Thus, the equilibrium slope can be expressed as:

$$\tan\beta_e = \frac{I_U - I_B}{I_U + I_B}\tan\varphi_m, \tag{16}$$

where

$$I_U = \frac{1}{T}\int_{t_s}^{t_m} (|\theta(t)|)^{3/2}\mathrm{d}t,$$

$$I_B = \frac{1}{T}\int_{t_m}^{t_e} (|\theta(t)|)^{3/2}\mathrm{d}t, \tag{17}$$

in which T is the wave period, t_s and t_e the start and end time of the swash oscillation, and t_m the moment at which uprush changes to backwash.

Klonaris et al. (2018) proved that the application of the latter quasi-empirical formulation is especially efficient in predicting swash morphodynamics, in conjunction with a phase resolving Boussinesq-type model, ensuring the continuity of sediment fluxes throughout the surf and swash zones and providing a smooth transition between them. The main advantage of this approximation is that the computed sediment transport rates do not decrease too rapidly from the swash to offshore zones, guaranteeing the stability of the solution throughout the entire coastal zone.

The investigation of sediment dynamics in this zone is of high interest for engineering applications. Swash dynamics determine the shoreline position, thus the precise evaluation of the natural processes in this zone contributes to the performance evaluation of coastal defense structures in terms of their capacity to maintain or advance the shoreline seaward. Hence, it is considered that combining a highly nonlinear Boussinesq wave model with a sophisticated representation of wetting-drying conditions, along with a quasi-3D sediment transport formula incorporating sediment fluxes in the swash zone is crucial in obtaining accurate bed level predictions in the presence of coastal engineering structures, therefore improving engineering design.

2.3. Morphology

Total sediment transport rates are computed as the sum of the bed and suspended loads in the intermediate depths and surf zone. In the swash zone, the sediment rates, estimated using Larson and Wamsley's (2007) approximation, are also added to the total sum of sediment fluxes in cross-shore and alongshore direction. The variables of FUNWAVE-TVD model have been used to estimate these rates following the time scale of hydrodynamic circulation. However, morphological changes vary at a different and slower rate compared to the short-term variations of hydrodynamics. Thus, the estimation of bathymetry update requires maintaining a budget of the sediment fluxes that have been derived by averaging the instantaneous flow parameters. Thus, these sediment transport fluxes were integrated over a number of time steps, which correspond to several wave periods. The bathymetry update was calculated by solving the sediment mass conservation equation which reads:

$$\frac{\partial z_b}{\partial t} = -\frac{\mathrm{Morfac}}{1-n_p}\nabla\cdot\boldsymbol{q}_{tot}, \tag{18}$$

where n_p is the sediment porosity, $\boldsymbol{q}_{tot} = (q_{tot,x}, q_{tot,y})$ denotes the total volumetric sediment transport rate equal to the sum of suspended and bed-load transport rate, z_b is the local bottom elevation and Morfac is a morphological acceleration factor (Lesser, 2004). This nonunity factor (Morfac) applies a scalar multiplier to the sediment continuity equation and speeds up the depth change rates, multiplying them by a constant value. In this study, Morfac values (ranging from 1 to 30) were systematically adapted to be compared with a baseline condition of no acceleration. Care must be taken not to exaggerate with extreme Morfac values, in order to describe realistically the interaction of the wave, hydrodynamic and morphology modules.

The effect of the bed slope on sediment transport has been included following Watanabe (1988). Following Leont'yev (1996) and Karambas et al. (2002) the sediment mass conservation equation can be obtained from

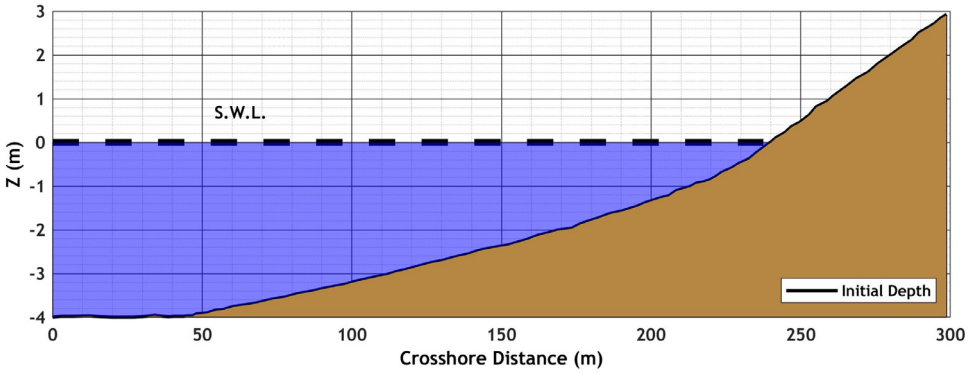

Figure 2 Initial beach profile setup in the Dette et al. (2002) experiments.

Equation (18) as follows:

$$\frac{\partial z_b}{\partial t} = -\frac{\partial}{\partial x}\left(q_{tot,x} - \varepsilon|q_{tot,x}|\frac{\partial z}{\partial x}\right) - \frac{\partial}{\partial y}\left(q_{tot,y} - \varepsilon|q_{tot,y}|\frac{\partial z}{\partial y}\right), \quad (19)$$

in which, ε is an empirical coefficient that varies within the range of 2.0 to 5.0. The second term in each of the parentheses in the right part of Equation (19) describes the diffusion term, as well as additional gravitational term reflects the effect of local bed slope on sediment transport.

3. Model validation

For the validation of the presented composite model, four different test cases were evaluated, both in 1DH and 2DH configurations. Our results were compared to experimental and numerical findings involving hydrodynamic, sediment transport loads and short and medium-term bathymetry changes. Taking advantage of FUNWAVE-TVD model's capacity to employ rapidly varying terrains and steep slopes in the surf zone, this study provides significant insights into the sediment transport dynamics in a variety of coastal engineering applications. Sediment transport and morphology evolution were analyzed for the case of large-scale wave flumes using the experimental findings of Alsina et al. (2012) and Dette et al. (2002). These test cases were also utilized for the calibration of several empirical factors and formulas, as the required computational cost for the performed simulations was significantly lower than that of the 2DH cases. Our numerical model was applied afterwards, in the case of the physical experiments of Badiei et al. (1995), concerning the effect of a groyne on the shore morphology. Ultimately, the effect of shore parallel emerged and submerged breakwaters on the hydrodynamics and morphology was evaluated. For this purpose, our numerical results were quantitatively compared to the empirical models from previous related studies (Bos et al., 1997; Cáceres et al., 2005; Deltares/Delft Hydraulics, 1997). Thus, the efficiency of the proposed coupled model was tested under real field dimensions and for a total duration of 50 days, providing significant conclusions about the time scale of the achieved morphological equilibrium.

Table 1 Summary of the retrieved experimental wave and bathymetry data from the study of Dette et al. (2002).

H_s (m)	1.20
T_p (s)	5.5
Water depth at wavemaker (m)	5.0
D_{50} (mm)	0.30
Total duration (h)	23
Bed slope	Varying

3.1. 1DH Surf and swash zone morphological processes in cross-shore direction

3.1.1. Large Wave Flume experiment

The first set of comparisons refers to the experimental campaign carried out at the Grosser Wellenkanal in Hannover within the context of the EU SAFE project. The results of this work were presented in the study of Dette et al. (2002). The main objective of that study was to investigate the effectiveness of beach nourishment as a soft protection technique to combat coastline erosion. The experiments were performed in a wave flume 324 m long, while the width and the depth of the flume were 5 m and 7 m, respectively. Figure 2 depicts a layout of the flume bathymetry. Herein, the test B2 of the experimental campaign was reproduced in order to evaluate the results of our numerical coupled model. Irregular waves were applied ($H_s = 1.20$ m and $T_p = 5.5$ s) using a TMA spectrum internal wavemaker (Wei and Kirby, 1999), for a total duration of 23 hours. The initial bathymetry was characterized by a horizontal bed of 5 m depth followed by the theoretical Bruun equilibrium profile (Bruun, 1954; Dean, 1977) below the water level. The sea bottom was represented by well-sorted sand with a median sediment size of $D_{50} = 0.30$ mm. A summary of the retrieved experimental wave and bathymetry data that were used as input for the numerical simulation is given in Table 1.

The bathymetry data were discretized on an equispaced grid with a spatial step of $\Delta\chi = 0.5$ m and a fixed bottom friction coefficient was utilized and set equal to $C_d = 0.008$, as it was found that it leads to the best agreement with the experimental data. The minimum water depth used to represent wetting-drying conditions was set equal to 0.01 m.

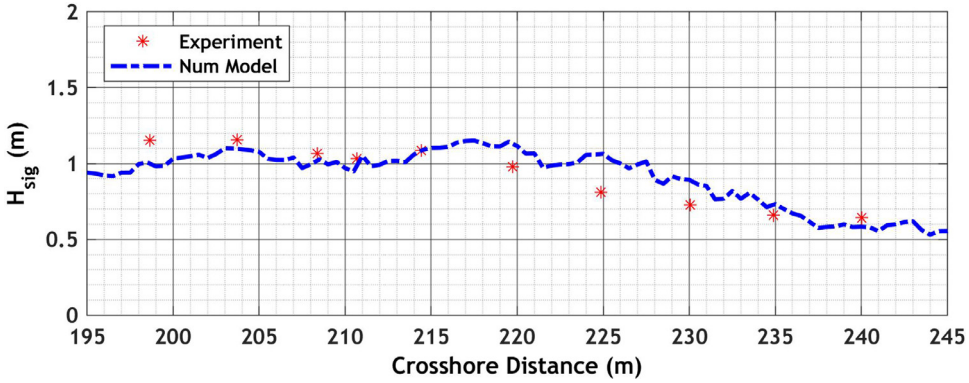

Figure 3 Computed and measured significant wave height after 19 h 45 min. of wave action for the test case B2 in Dette et al. (2002).

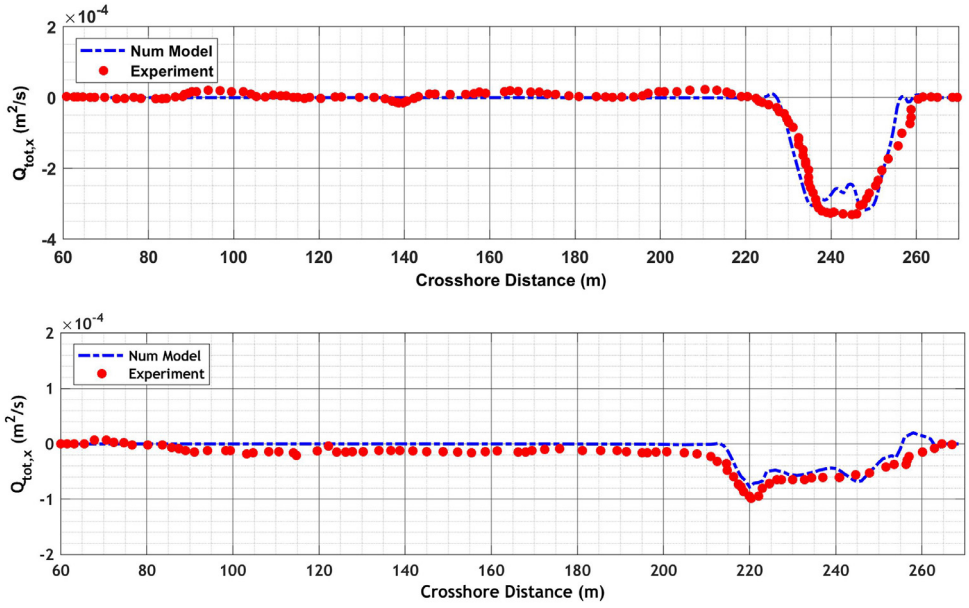

Figure 4 Computed and measured total sediment transport rate after 1.5 h (up) and after 19 h 45 min. (down) for the test case B2 in Dette et al. (2002).

The selected Courant number in the time-stepping scheme of the FUNWAVE-TVD model was relatively low (CFL = 0.3) to achieve numerical stability. A low morphological factor was utilized (Morfac = 2) to ensure the stability of the numerical simulation and calibrate the sediment transport model. The empirical coefficient ε of Equation (19) was set equal to 5, in order to represent the effect of the bed slope on seabed morphology. The applied settling velocity w_s was equal to 0.0267 m/s, with sand porosity $n_{p=}$ 0.4.

Figure 3 shows the distribution of significant wave height along the flume profile and the comparison between the computed and measured data for the test B2 of Dette et al. (2002). Computed and measured values of sediment transport rates and seabed geometry are depicted in Figures 4 and 5, respectively. The wave height distribution was accurately computed using FUNWAVE-TVD model taking advantage of its high order nonlinearity. Moreover, the sediment transport model reproduced adequately the peaks of the sediment load distribution along the cross-shore profile. The bar formation is well predicted, although the model overestimates the shoreline erosion in the swash zone.

3.1.2. SANDS experiment

This test case refers to the Hydralab III SANDS project (Scaling and Analysis and New instrumentation for Dynamic bed testS). The experiment was carried out in the Canal de Investigacion y Experimentacion Maritima (CIEM) at the Universidad Politecnica de Cataluña (UPC), Barcelona. The dimensions of the large-scale wave flume were: 100m long, 3m wide and 4.5 m deep. Figure 6 shows a snapshot of the initial bathymetry in the laboratory flume. The experimental findings were presented in the study of Alsina et al. (2012). The main purpose of this physical experiment was to investigate the link between swash zone dynamics and surf zone morphodynamics and how dissipative beaches with mild-sloping beach face tend to decrease the rate of sand bar migration towards the sea, while more reflective swash conditions intensify sediment transport erosive rates.

During the experiment, moderately energetic random waves were applied (H_s = 0.53 m and T_p = 4.14 s) and the same wave conditions were repeated for a series of 47 tests. Each test was comprised of 500 waves with a to-

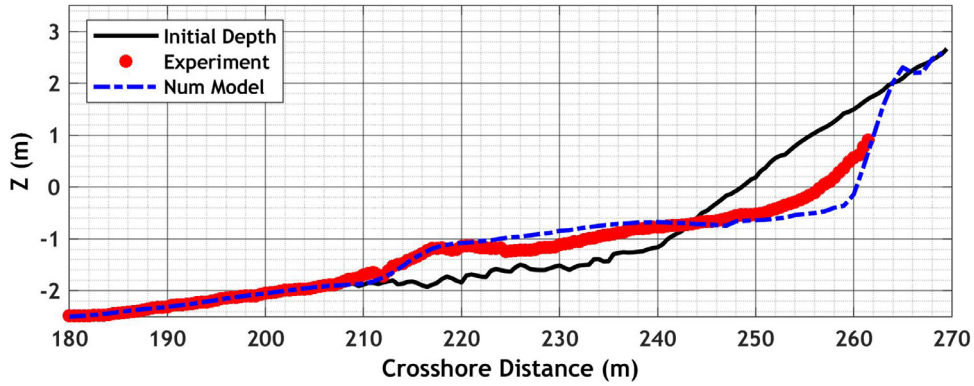

Figure 5 Computed and measured bottom elevation after 19 h 45 min. of wave action for the test case B2 in Dette et al. (2002).

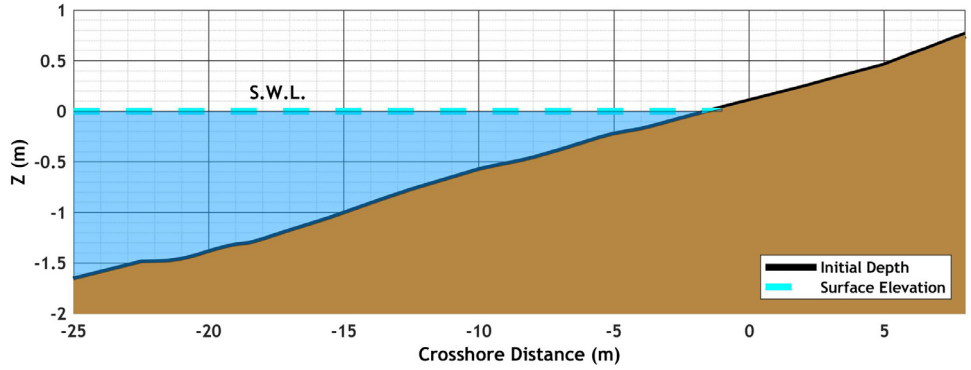

Figure 6 Initial beach profile used for SANDS experiment (Alsina et al. 2012).

Table 2 Summary of the retrieved experimental wave and bathymetry data from the study of Alsina et al. (2012).

H_s (m)	0.53
T_p (s)	4.14
Total duration (h)	21.15
Water depth at wavemaker (m)	2.47
D_{50} (mm)	0.25
Bed slope	1:10

tal duration equal to 27 min. The random wave time series corresponded to a JONSWAP spectrum with a peak factor of $\gamma = 3.3$. The initial bathymetry was characterized by a constant sloping beach with a gradient of 1:10. The sea bottom was represented by well-sorted sand with a median sediment size $D_{50} = 0.25$ mm. A summary of the retrieved experimental wave and bathymetry data that were used as input for the numerical simulation is given in Table 2.

In order to reproduce the experimental procedure numerically, the bathymetric data were interpolated on a fine grid with a spatial step of $\Delta x = 0.2$ m. The initial bathymetry consisted of a horizontal bottom of 2.47 m depth followed by a uniform slope of 1:10. A fixed bottom friction coefficient (C_d) was utilized and set at 0.009 and the minimum water depth for wetting-drying conditions was considered equal to 0.01 m. Once again, the Courant number used in the time-stepping scheme of the FUNWAVE-TVD model was relatively low ($CFL = 0.3$) in order to achieve numerical stability. No morphological acceleration factor (Morfac = 1) was employed, as the total simulation time was relatively low (Duration= 21.15h). Similar wave conditions to that of the experiment were generated ($H_s = 0.53$ m and $T_p = 4.14$ s) by an irregular wavemaker in a water depth of 2.47 m, producing a JONSWAP spectrum. The empirical coefficient ε of Equation (19) was set equal to 5. in order to consider the impact of the bed slope on seabed morphology. The applied settling velocity w_s was equal to 0.0267 m/s, with sand porosity $n_p = 0.4$.

The initial computed and measured cross-shore distribution of significant wave height after 21.15 hours of wave action are both depicted in Figure 7. The initial beach profile, as well as the computed and measured final beach profiles at 21.15 hours, are also shown in Figure 7. The present test case corresponds to erosive conditions close to the swash zone due to the initial reflective beach profile that, in turn, force significant sediment quantities into deeper water. FUNWAVE-TVD model estimated accurately the cross-shore wave height distribution due to its higher order of nonlinearity. However, it should be noted that some discrepancies between measurements and numerical results appear in the area where water depth is less than 0.5 m. A breaking event takes place just after $x = -20$ m leading to the formation of the inner bar.

The numerical outputs of the sediment transport model are in good agreement with experimental results, as an accurate prediction of the sandbar formation was achieved. Overall, the evolution of the bed shape over time follows

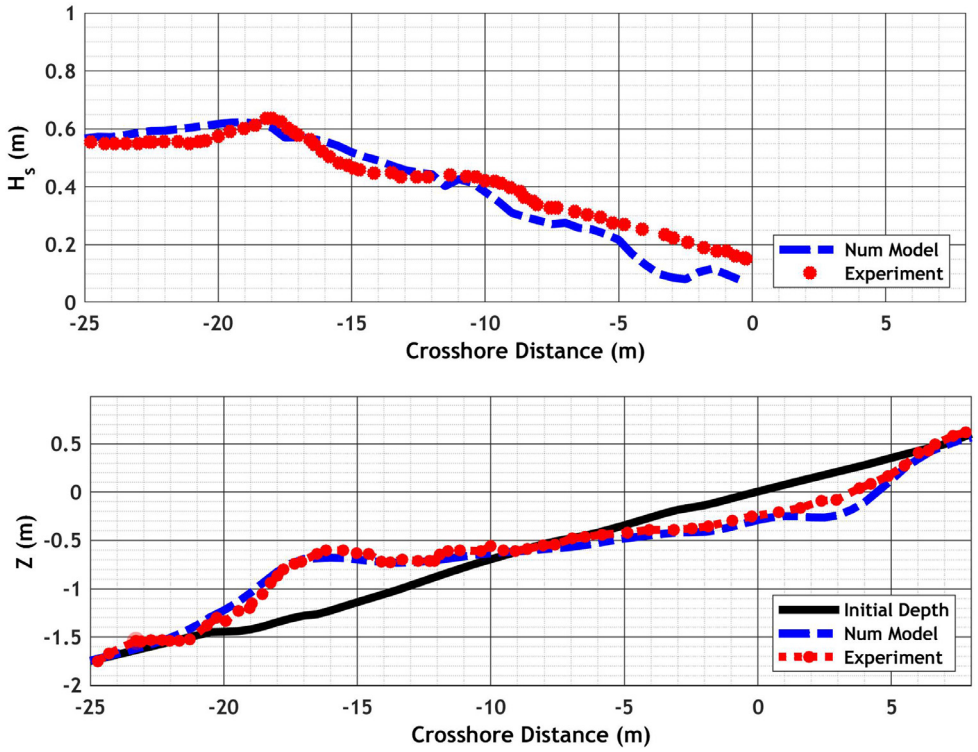

Figure 7 Computed and measured cross-shore distribution of significant wave height after 21.15 hours (top panel). Computed and measured final beach profile after 21.15 hours (bottom panel).

the same sequence as that of the experiment, since a seaward sandbar migration was observed. However, a bed-change over-estimation of $\pm$ 0.10 cm can be detected in the swash and surf zone.

3.2. 2DH numerical simulations for the effect of a single groyne structure on the shore

The impact of a groyne structure, which acts as an artificial obstacle to the longshore sediment transport and affects the subsequent shoreline evolution, was numerically investigated in our study and compared with the experimental findings of Badiei et al. (1995). Single groynes are referred to as the structures that are usually placed normal to the shoreline and block the littoral drift partially or completely (Kristensen et al., 2016). Groynes are employed to produce sediment cells in which the shore can turn against the locally predominant wave direction. These structures can also be situated close to a river mouth to aid the canalization of the flow into the sea (Valsamidis et al., 2017), or as terminal structures (jetties) which limit the amount of sediment, deposited in the harbor basin. An accretive or erosive trend is expected to occur in the vicinity of a groyne due to the presence of a source or sink, respectively. Moreover, in coastal management, a system of multiple groynes is typically used to advance the shore seaward and trap large amounts of sediments by blocking alongshore sediment fluxes. Thorough research of groyne system functionality was conducted by French (2001).

The physical model presented by Badiei et al. (1995) concerns nearshore sediment transport dynamics and morphological effects of groynes on a mobile bed with an initial straight beach, which was exposed to obliquely incident irregular waves at an angle of 11.6 degrees (with respect to the shore-normal). The test NT2 of the experimental study was reproduced numerically in the scope of the present work. The median particle diameter of bed material (D_{50}) was 0.12 mm and the initial cross-shore constant beach slope was 1:10.

The integrated coupled model was applied to reproduce the hydrodynamic and morphodynamic conditions of the experiment. The spatial domain has been discretized with a spatial step of $\Delta x = 0.2$ m and $\Delta y = 0.5$ m in cross-shore and alongshore direction, respectively. Irregular waves (characterized by a JONSWAP spectrum at the wave-maker), were generated with $H_s = 0.8$ m and $T_p = 1.15$ s, whilst the angle between the normal to the coast and the main direction of wave propagation was set at 11.6°. For the absorption of the wave energy propagating out of the model area, a sponge layer of about 5 m was applied at the offshore boundary of FUNWAVE-TVD model and periodic lateral boundary conditions were employed. In Figure 8, the initial bathymetry with a constant slope of 10:100 is illustrated. The wave-maker was placed at X = 7 m and in the deepwater region a flat bottom of 2 m was considered. The total duration of the simulation was 12 hours, equal to that of the experiment and a morphological acceleration factor in the order of 5 was employed. The applied settling velocity w_s was equal to 0.0084 m/s, with sand porosity $n_p = 0.39$.

Figure 9 depicts the wave-induced current field after 1 hour of wave action. The groyne structure alters the longshore currents' direction in its vicinity, as decreased velocities can be seen in the lee side of the structure.

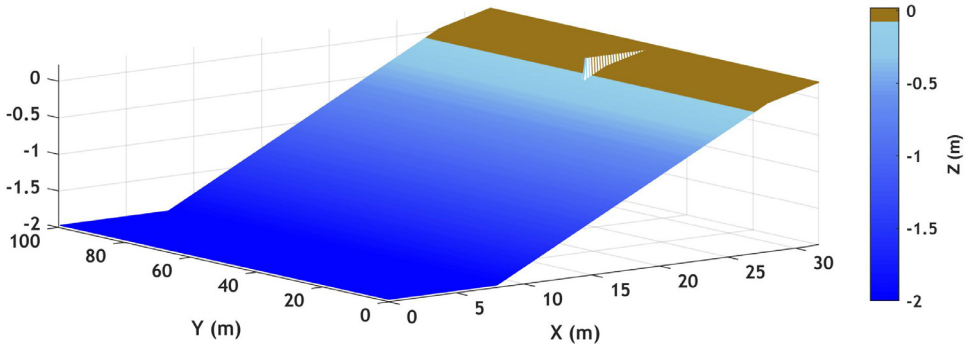

Figure 8 3D view of model's initial bathymetry.

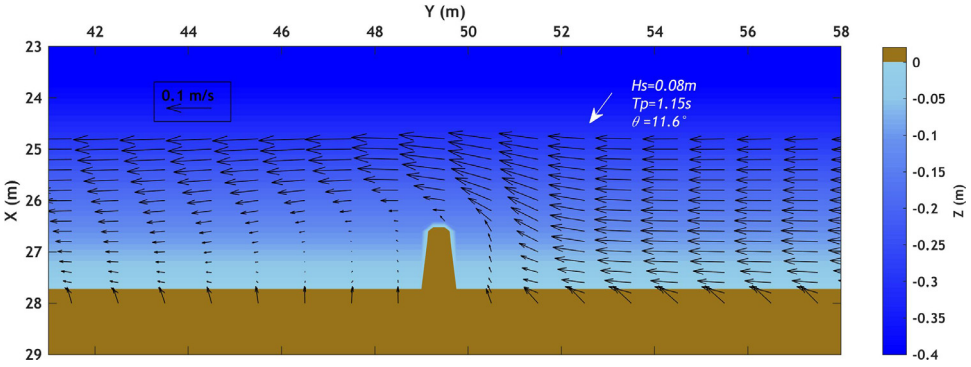

Figure 9 Simulated hydrodynamic circulation after 1 hour of wave action for a groyne field subject to waves with a 11.6° angle of incidence. Color map corresponds to the initial bathymetry.

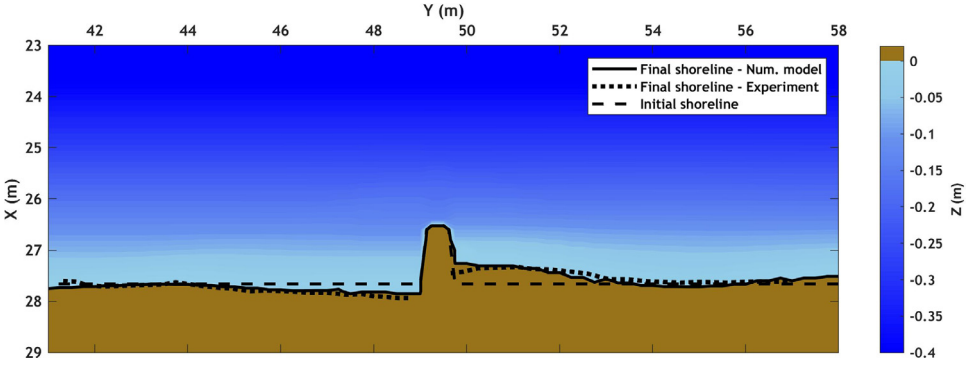

Figure 10 Simulated bathymetry for a groyne field subject to waves with a 11.6° angle of incidence depicting the measured (dotted line) and computed (solid line) final shoreline position. Color map indicates the final bathymetry.

The nearshore currents reach a maximum velocity of about 0.1 m/s. Moreover, offshore-oriented velocities are observed in the swash zone, reflected from the beach face, with a maximum velocity of 0.06 m/s. The direction and order of magnitude of computed currents are in line with the numerical findings of the study of Karambas and Samaras (2017), in which the present experimental test case was also reproduced. However, reflection phenomena in the vicinity of groyne are less intense in our study, due to the application of inner sponge layers that represent flow friction and energy dissipation within the structure.

Figure 10 shows the final bottom evolution after 12 hours of wave action. The sediment accretion updrift of the structure contributes to an advance of the shoreline seaward, whilst the lack of sediments at the lee side of the structure results in a shoreline retreat. Overall, the numerical findings are in very good agreement with the experimental results, as is evident in Figure 10. The computed final shoreline position is almost identical to that of the experiment, with some small discrepancies encountered close to the lateral boundaries.

3.3. 2DH numerical simulations for the effect of a detached breakwater on the shore

3.3.1. Single emerged breakwater

To provide significant protection against erosion phenomena in the littoral environment, layout optimization of a breakwater is necessary. Previous studies have revealed that breakwater geometry affects hydrodynamic processes and evolution of bottom topography, resulting in a plan form

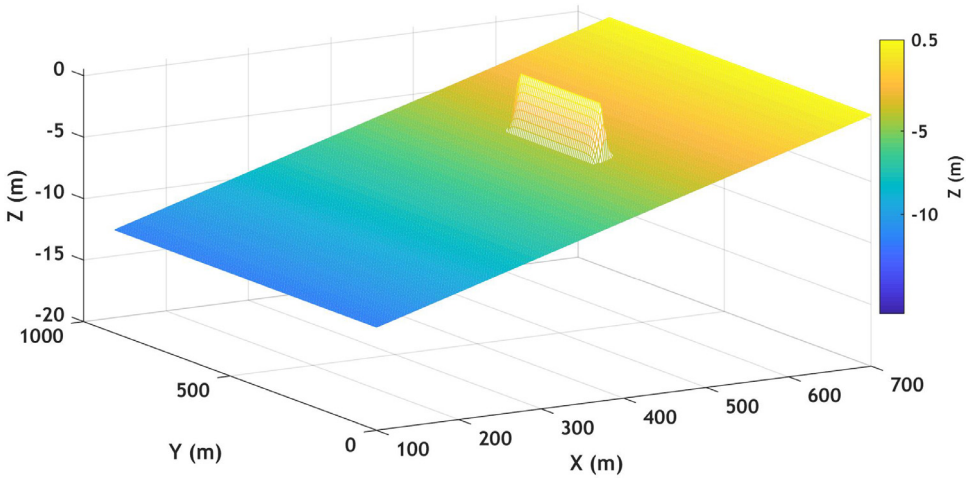

Figure 11 3D illustration of the initial bathymetry (breakwater at 200 m from shore).

development (formation of tombolo or salient) in the lee of the breakwater (Bos et al., 1997; Cáceras et al., 2005; Deltares/Delft Hydraulics, 1997; Zyserman et al., 2002). The type of beach plan form strongly depends on the dimensions and location of the structure. In the case of emerged detached breakwaters, the beach can extend and come in contact with the structure (formation of tombolo). Permanent tombolo is expected for L/D $>$ 1 and salient for L/D $<$ 1 according to Van Rijn (2011) with L being the breakwater length, and D being the offshore distance to the original shoreline. However, the morphological evolution in the lee of breakwaters is a complex physical process that cannot be analyzed in terms of only two parameters (L, D). The beach response relies on several environmental factors, such as three-dimensional bathymetry characteristics, prevailing hydrodynamic conditions and sediment supply. Additionally, geometric properties of the structure, including freeboard, structure slopes, crest width, length of the gap between segments of the breakwater system, and breakwater porosity are known to be influential in beach morphology (Afentoulis et al., 2019).

Deltares/Delft Hydraulics (1997) and Bos et al. (1997) carried out a study about the effect of a detached emerged breakwater on coastal hydro-morphodynamics, using numerical modeling approaches. Herein, this work is used as a benchmark test for the validation of our numerical model in field conditions. This application is of high interest, as the model's behavior may vary from laboratory to field dimensions. It has been revealed that the achievement of moveable bed equilibrium is slower in the field than in the laboratory's controlled conditions, where the use of lightweight sediment can introduce additional scale effects (Gorrick and Rodríguez, 2014). Hence, the present test case corresponds to a total duration of 50 days, which is deemed a sufficient period to explore the model's capacity to capture fluid-seabed interactions over a relatively larger time scale.

The examined test case consisted of 300 m long breakwater with a crest height of $+0.5$ m, located on an initially along-shore uniform sloping bottom, with a slope of 1:50 and placed at 200 m offshore the shore. In order to reproduce this test case numerically, the bathymetric data were interpolated over a rectangular grid with a spatial step of $\Delta x = 2$ m and $\Delta y = 5$ m in cross-shore and alongshore direction, respectively. Irregular waves were generated with $H_{rms} = 2.0$ m and $T_p = 8.0$ s. Fine sand was considered with median sediment size $D_{50} = 0.25$ mm. The applied settling velocity w_s was equal to 0.0267 m/s, with sand porosity $n_p = 0.41$ and the selected Courant number in the time-stepping scheme of the FUNWAVE-TVD model was CFL $=$ 0.45. A sponge layer 100 m wide was applied at the offshore side to absorb the reflected waves from the breakwater. The dissipation of wave energy at the breakwater location was achieved using large bottom friction locally (a high drag coefficient of $C_d = 10$ was considered) and periodic lateral boundary conditions were applied. A morphological acceleration factor (Morfac $= 30$) was employed to reduce the relatively high computational cost. The morphological acceleration option was activated after 7 days of wave action when quasi-steady flow conditions prevailed. In Figure 11 the initial bathymetry along with the breakwater configuration is illustrated.

Figure 12 shows a snapshot of the computed instantaneous free surface elevation. The nearshore processes that can be identified in this Figure are the wave shoaling, diffraction into the sheltered area as well as run-up and run-down. The wave breaking over the breakwater can be observed at X $=$ 400 m. Subsequently, Figure 13 depicts the mean sea level during the 1st hour of wave action. Wave set-up of about 0.08m can be observed in the lee part of the breakwater and in the illuminated area due to the wave-induced flux nearshore.

The initial wave-induced current field after 1 hour of wave action, superimposed with bathymetry contours, is depicted in Figure 14. A formation of two eddies can be observed in the lee of the breakwater. The generation of eddies is due to the current circulation towards the sheltered area, parallel to the shoreline and across both sides. This formation is generated due to the gradient of the mean sea level between the illuminated area and the sheltered area, which leads to diffraction effects with a consequent forcing of currents towards the down-wave of the structure (Karambas, 2012). Additionally, weak rip currents with a velocity of about 0.2 m/s can be identified between the

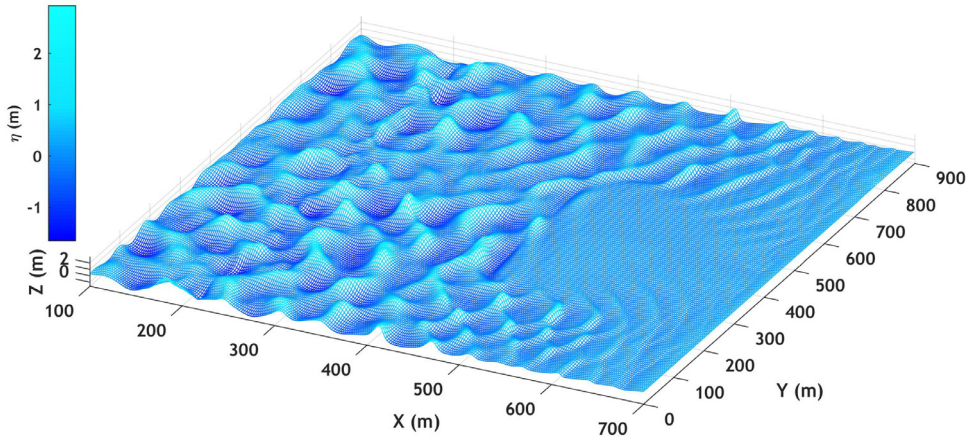

Figure 12 Snapshot of the instantaneous computed free surface elevation.

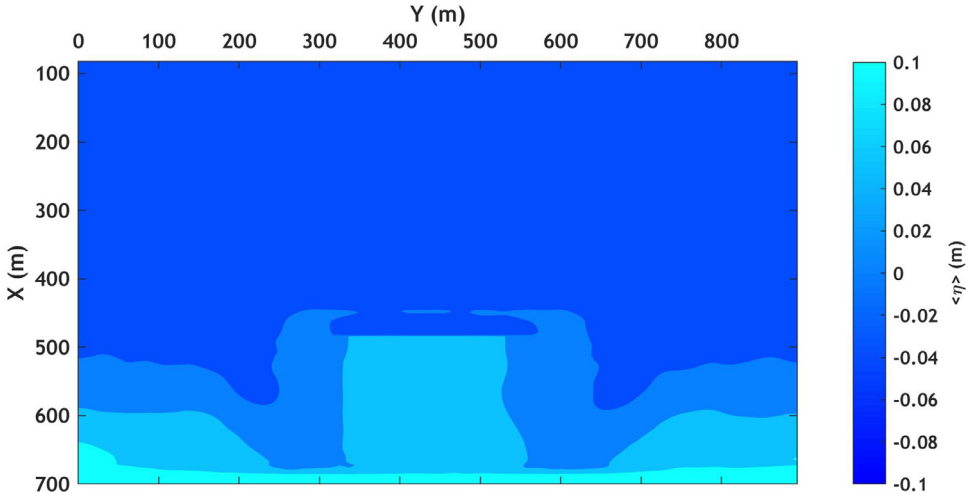

Figure 13 Mean surface elevation during the 1st hour of wave action.

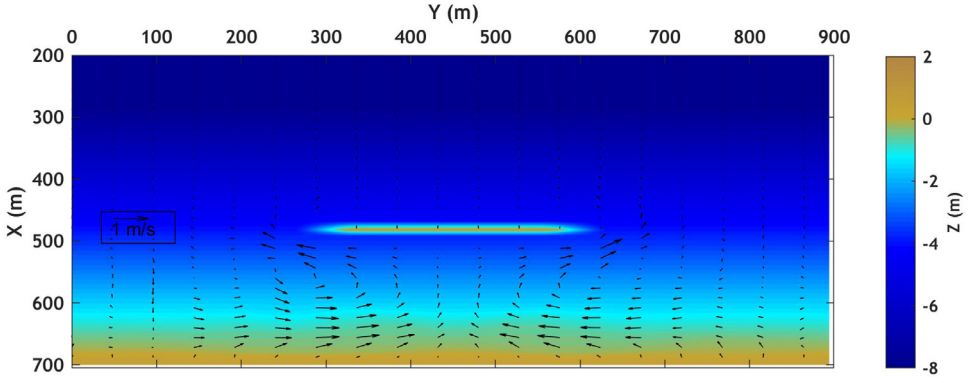

Figure 14 Simulated hydrodynamics after 1 hour of wave action. Colors: initial Bathymetry, vectors: calculated wave induced current intensity and direction.

lateral boundaries of the model and the structure, while offshore-oriented velocities are detected close to the shore, reflected from the beachface with a maximum velocity of 0.75 m/s.

Figure 15 shows the wave-induced current field after 1 day of wave action, superimposed with seabed changes during this time. The seabed evolution is more intense in the zones where significant spatial velocity gradients occur. The developed plan form results in a shortening in the shore-normal direction of the two eddies, which are shifted towards the two gaps, with a slight decrease of the relevant velocities compared to the initial current field. Close to the shore, the seaward oriented currents resulted in the altering of the uniformity of the beach in the alongshore direc-

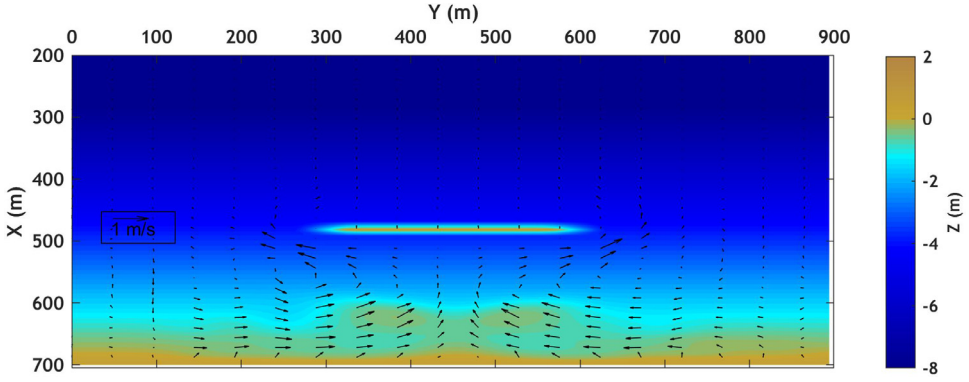

Figure 15 Simulated morphodynamics after 1 day of wave action. Colors: sea bed elevation, vectors: calculated mean wave induced current intensity and direction.

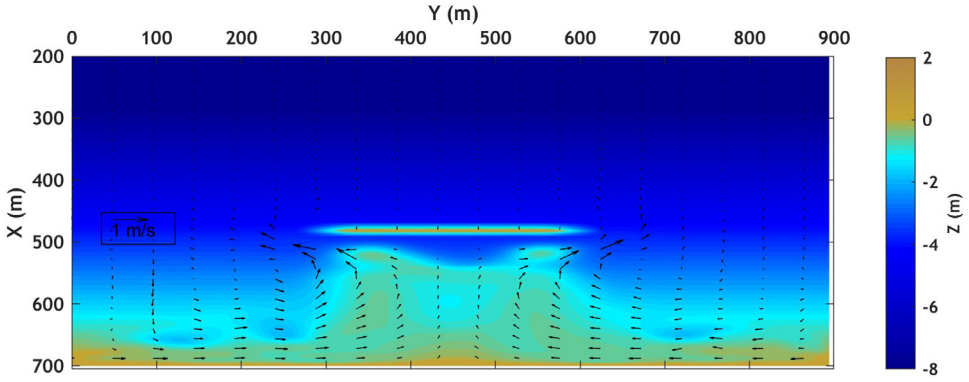

Figure 16 Simulated morphodynamics after 10 days of wave action. Colors: sea bed elevation, vectors: calculated mean wave induced current intensity and direction.

tion, with associated erosion conditions. Figure 16 shows the seabed elevation after 10 days of wave action and the associated wave-induced currents. Behind the structure, the shoreline extends out and a tombolo starts to be formed. It should be mentioned that the initial geometry with a cross-shore constant slope is not realistic, thus the wave-current-seabed system tends to find equilibrium by altering the beach slopes near the shoreline. Therefore, dissipative conditions are observed in the foreshore beach morphology after 10 days and the computed erosion of the beach face at both sides is about 1m. This three-dimensional beach form forces alongshore nearshore currents with a magnitude of 0.3 m/s. In addition, strong rip currents with a magnitude of about 0.9 m/s are detected in the vicinity of the breakwater.

The bathymetry obtained after 50 days of wave action is illustrated in Figure 17. It can be observed that no significant differences in sea bottom geometry take place between 10 and 50 days. It is concluded that the rate of bottom level change was high initially and slowed down as equilibrium approached. Close to the equilibrium stage, relatively weak velocities of about 0.3 m/s characterize the wave-induced current field. During this phase, the waves break out of the shadow zone due to the presence of the tombolo, resulting in a less energetic current field in the protected area. Consequently, since the current velocities are relatively weak, the sediment fluxes are insignificant and there is no noticeable change of the seabed geometry.

The agreement between the obtained results and the corresponding retrieved data of the study of Deltares/Delft Hydraulics (1997) seems quite satisfactory, concerning the accretion close to the center-line of the wave tank and the observed erosion of the beach face at both sides. Overall, a formation of tombolo was achieved for $L/D > 1$, which is in line with the available field data used in the study of Deltares/Delft Hydraulics (1997). Furthermore, the outcome of our numerical investigation is consistent with the computed bottom evolution and hydrodynamics revealed in the study of Razak et al. (2018), concerning a similar test case. Razak et al. (2018) used XBeach model to assess beach response in the lee part of breakwater under the same wave conditions as that used in our study. Once again, a single tombolo was formed after 50 days of wave action whilst the computed currents followed flow patterns (discrete vortices) close to our estimates.

3.3.2. Single submerged breakwater

The proposed coupled model was utilized to investigate the hydrodynamic and morphodynamic patterns as well as the beach morphology in the vicinity of a submerged offshore breakwater. These structures lead in wave energy reduction through depth-induced wave breaking and the shoreline response to submerged breakwater is gov-

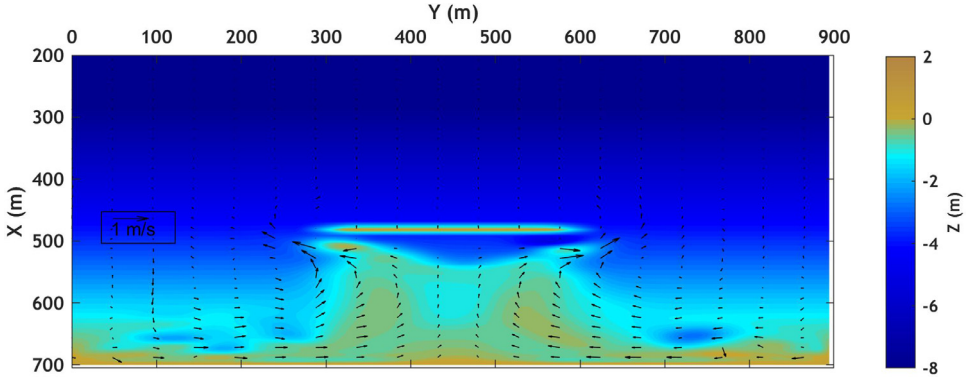

Figure 17 Simulated morphodynamics after 50 days of wave action. Colors: sea bed elevation, vectors: calculated mean wave induced current intensity and direction.

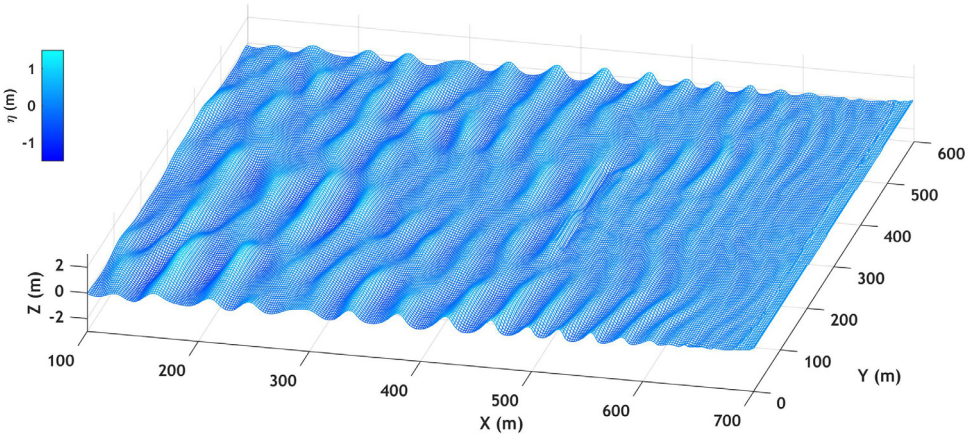

Figure 18 Snapshot of the instantaneous computed free surface elevation.

erned by hydrodynamic processes such as wave setup, wave set-down, onshore mass flux, and nearshore currents (Ranasinghe et al., 2010). The effect of structure freeboard is also dominant in shaping hydrodynamic patterns shoreward of the breakwaters. When a submerged breakwater is located close to the beach, strong erosion behind the structure appears and high turbulence levels occur due to wave breaking associated with high sediment suspension, which can be driven outwards the sheltered area by diverging fluxes (Tsiaras et al., 2020). Thus, potential erosion could occur in the case of short structure distances relative to the shore. Cáceres et al. (2005) used numerical modeling approaches, based on a phase averaged wave driver, to investigate the bed evolution behind low-crested structures. The effect of structure freeboard and significant wave height were thoroughly analyzed.

In order to evaluate the effect of submerged structures on beach morphology, the study of Cáceres et al. (2005) was utilized as a benchmark case. A smooth cross-shore slope, around 2:100, characterized the seabed and the bathymetric data were interpolated over a rectangular grid with a spatial step of $\Delta\chi = 2$ m and $\Delta y = 4$ m in cross-shore and alongshore direction, respectively. Irregular waves were generated with $H_{rms} = 1.0$ m and $T_p = 4.0$ s with a shore-normal direction. The breakwater crest height was set at -0.5 m (freeboard $= 0.5$ m) and the structure was placed in a distance of 230 m to the shore. The bottom evolution was computed for a duration of 200 hours and a morphological acceleration factor (Morfac $= 15$) was employed to reduce the computational cost. No sponge layers were employed in the location of the structure to simulate the depth-induced wave breaking and discharge flux over the submerged breakwater. Fine sand was considered with median sediment size $D_{50} = 0.25$ mm. The applied settling velocity w_s was equal to 0.0267 m/s, with sand porosity $n_p = 0.41$ and the selected Courant number in the time-stepping scheme of the FUNWAVE-TVD model was CFL $= 0.45$.

In Figure 18, a snapshot of the free surface elevation is illustrated. It can be observed that some wave breaking is initiated on the breakwater crest at X $= 470$ m while a portion of incident wave energy is reflected from the front breakwater face. The transmission of waves from the downstream side of the breakwaters is highly nonlinear, where free and bound transmitted waves travel into the shore (Christou et al., 2008). Nearshore phenomena such as wave shoaling, diffraction, run-up and run-down can also be identified in Figure 18. In contrast to emerged structures, submerged breakwater leads to wave transmission and overtopping. These processes can be reproduced more accurately through the highly nonlinear phase-resolving wave driver proposed in this study in contrast to the phase-averaged one utilized in Cáceres et al. (2005). Thus, the net mass transport that occurs above the structure increases wave-setup in the lee zone, which in turn forces outward rip currents around the heads of the structures and through the gaps.

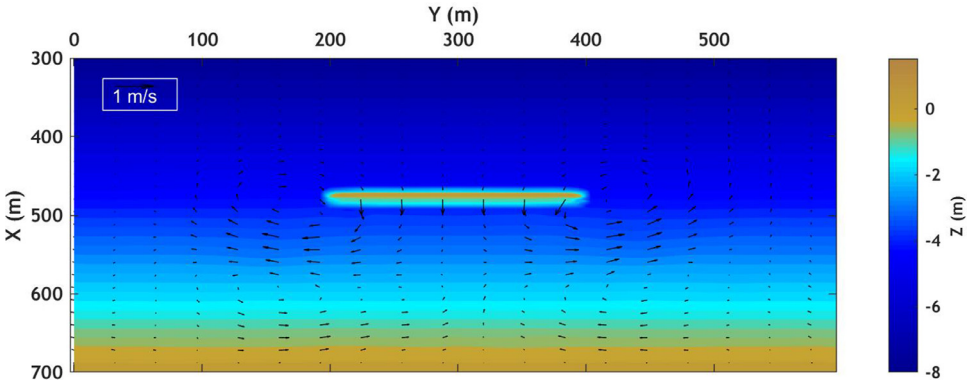

Figure 19 Simulated hydrodynamics after 1 hour of wave action. Colors: initial bathymetry, vectors: calculated wave induced current intensity and direction.

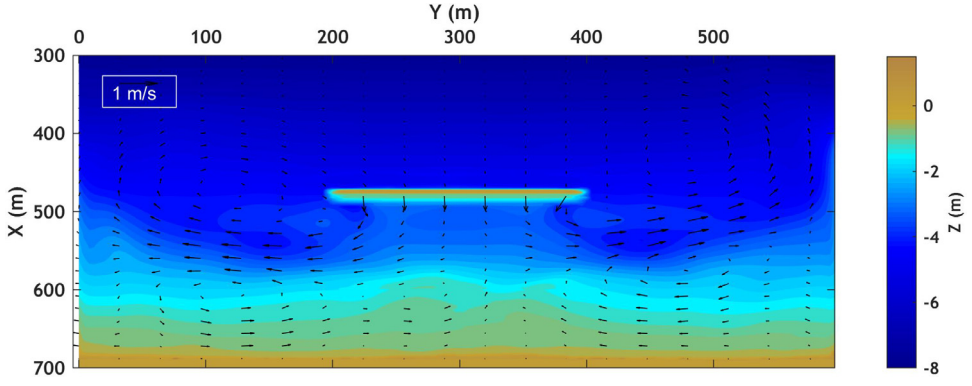

Figure 20 Simulated hydrodynamics after 200 hours of wave action. Colors: final bathymetry, vectors: calculated wave induced current intensity and direction.

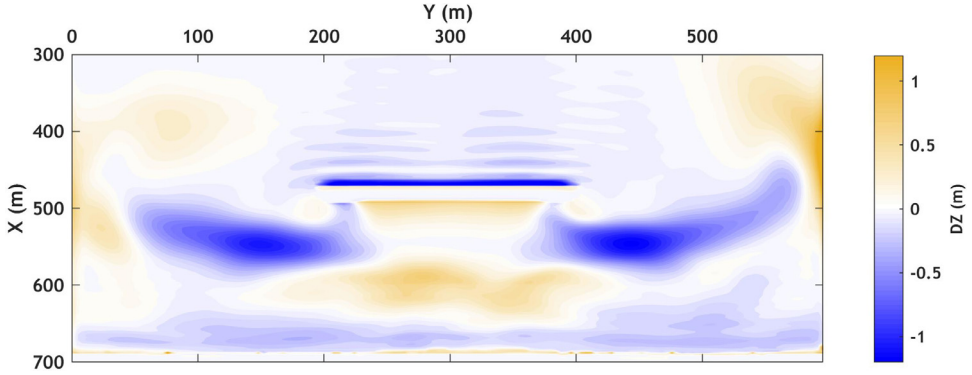

Figure 21 Simulated seabed changes after 200 hours of wave action. Colors: Seabed level changes (Dz).

Figure 19 presents seabed geometry and the wave-induced current field after one hour of wave action. Two symmetric eddies can be identified associated with strong currents of about 0.8 m/s. This is in line with the other studies, which have revealed that the dominant source of vorticity, in the case of submerged breakwaters, is located around the edges of the structure (Bouvier et al., 2019). In contrast to the case of the emerged breakwater, the nearshore vortex is hindered, and the order magnitude of nearshore velocities is relatively low, of about 0.3 m/s. This is due to the fact that the overtopping flux extends in a limited area around the structure and governs the circulation, suppressing the nearshore currents.

The computed bathymetry and the associated wave-induced current field after 200 hours of wave action are presented in Figure 20. The model results are in good agreement with the findings of Cáceres et al. (2005), as the integrated model succeeded in reproducing all morphological and hydrodynamic patterns behind the breakwater and up to the shore. Once again two symmetric eddies can be identified outside of the sheltered area, while strong diverging erosive currents, with a velocity of 0.8 m/s, prevail through the gaps. The overall bottom evolution reveals erosion close to the structure, while the shoreline is accreting, and the formation of salient can be observed. Figure 21 illustrates computed bottom elevation changes after 200 hours of wave

action. The predicted bed-level accretion in the sheltered area is about 1 m, whilst intense erosion of 1.2 m can be identified in the zone where erosive diverging currents appear. Furthermore, slight bed level erosion of 0.3 m can be observed close to the swash zone.

4. Conclusions

In the present paper, a newly developed sediment transport model was introduced and coupled to a highly nonlinear Boussinesq wave model in order to assess the combined effect of waves and currents and ultimately the bed level evolution of coastal areas. Special attention was given to the swash zone dynamics which are considered dominant in shaping the morphological bed level changes, as well as to the unsteady wave effects on the bed load sediment transport rates. The combination of the sophisticated Boussinesq model along with a quasi-3D sediment transport model incorporating swash zone dynamics is considered to be extremely valuable in obtaining accurate bed level predictions in complex coastal areas. Of particular interest was the investigation of the interaction between hydrodynamics, seabed and coastal structures, with the obtained results having strong implications on the improvement of the structures' design and performance in protecting the shoreline.

The model was validated against the experimental data of Alsina et al. (2012) and Dette et al. (2002) in order to assess seabed morphology in the inner and swash zone. The prediction of erosion or accretion close to the shoreline is crucial for engineering applications and can affect the solution throughout the whole computational domain. The effect of swash zone dynamics was embedded, and the good agreement between model results and laboratory measurements enhance the robustness of our numerical approach. For the evaluation of the morphological influence of groyne structures, the physical experiment of Badiei et al. (1995) was reproduced. The numerical model results are in very good agreement with the experimental findings in the context of an accurate prediction of the measured bed evolution and shoreline position. Moreover, the performance of the composite model was evaluated in terms of its capacity to estimate the effects of detached emerged and submerged breakwaters on morphological features under real field conditions. The computational results were quantitatively compared to those of other studies (Cáceres et al., 2005; Deltares/Delft Hydraulics, 1997) and a good agreement was achieved. The formation of tombolo/salient was reproduced accurately and was found to be in agreement with the limits defined in the literature.

Regarding the several parameters/coefficients that utilized in this research, special attention should be given to the choice of the empirical coefficient of Equation (19), where values up to 3 should be employed for intermediate beaches and up to 5 for reflective beach profiles, in order to represent avalanching phenomena associated with steep slopes. This element was proven particularly important in order to guarantee the stability of the numerical simulations and the accuracy of the final solution, in combination with a properly selected time step of the continuity equation (Exner), which was set equal or slightly higher than the corresponding one, used in hydrodynamic simulations. Furthermore, the application of periodic boundary conditions allowed us to obtain a realistic wave-induced current field and minimize boundary effects in 2DH simulations. In addition, the acceleration techniques utilized in this research were significantly effective to reduce the computational burden, although a sensitivity analysis that was carried out herein, revealed that the values of the nonunity factor (Morfac) greater than 30 affects unrealistically the hydrodynamic solution. In the absence of clearly defined limits in the literature, Morfac values were adopted with particular caution in this work by performing trial and error simulations of a few hours, to define the upper allowable values of Morfac. This analysis served to consider non-linear morphological responses to wave forcing, and obtain a good compromise between simulation speed and accurate results.

In this study, swash and nearshore morphodynamics were investigated over dissipative and reflective beaches, as well as in transition profiles between the two states, where the formation of wave-breaking induced sandbars under the shoreface was accurately predicted, especially in the case of 1DH applications that allow us to assess small-scale physical processes. Although, further investigations are needed to model sand ripple morphology using finer grids and accretive wave sequences during the transition from reflective to dissipative beach states, knowing that the simulation of nearshore accretion phenomena is generally a more demanding task that requires the implementation of groundwater processes. Moreover, in order to extend the limitation of the present numerical approach, the role of aeolian sediment transport has to be considered in case of dune erosion and further benchmark test cases need to be evaluated, including estuary dynamics and gravel beaches.

Considering all the above, it is believed that the presented integrated model can be a valuable asset for engineers and scientists desiring to obtain accurate bed level evolution predictions in complex bathymetries with the presence of a variety of coastal protection structures, both in experimental and in field cases thus improving their design and configuration.

Declaration of competing interest

The authors declare that they have no known competing financial interests or personal relationships that could have appeared to influence the work reported in this paper.

References

Afentoulis, V., Eleftheria, K., Eleni, S., Evangelos, M., Archontia, L., Christos, M., Vasiliki, T., 2017. Coastal Processes Assessment Under Extreme Storm Events Using Numerical Modelling Approaches. Environ. Process. 4 (3), 731—747. https://doi.org/10.1007/s40710-017-0253-8

Afentoulis, V., Chini, N., Bardey, P., Raffourt, C., 2019. Sea bed evolution in the vicinity of longitudinal submerged discontinuous breakwaters — Acripelagos. International Scientific Conference on Design and Management of Harbor, Coastal and Offshore Works Athens, Greece.

Alsina, J.M., Cáceres, I., Brocchini, M., Baldock, T.E., 2012. An experimental study on sediment transport and bed evolution under different swash zone morphological conditions. Coast. Eng. 68, 31—43. https://doi.org/10.1016/j.coastaleng.2012.04.008

Badiei, P., Kamphuis, J.W., Hamilton, D.G., 1995. Physical experiments on the effects of groins on shore morphology. In: Proceedings of the Coastal Engineering Conference. https://doi.org/10.1061/9780784400890.129

Benoit, M., Marcos, F., Becq, F., 1997. Development of a third generation shallow-water wave model with unstructured spatial meshing. In: Proceedings of the Coastal Engineering Conference, 465—478. https://doi.org/10.1061/9780784402429.037

Birben, A.R., Özölçer, I.H., Karasu, S., Kömürcü, M.I., 2007. Investigation of the effects of offshore breakwater parameters on sediment accumulation. Ocean Eng. 34 (2), 284—302. https://doi.org/10.1016/j.oceaneng.2005.12.006

Bos, K.J., Roelvink, J.A., Dingemans, M.W., 1997. Modelling the impact of detached breakwaters on the coast. In: Proceedings of the Coastal Engineering Conference. https://doi.org/10.1061/9780784402429.157

Bouvier, C., Castelle, B., Balouin, Y., 2019. Modeling the impact of the implementation of a submerged structure on surf zone sandbar dynamics. J. Mar. Sci. Eng. 117 (4). https://doi.org/10.3390/jmse7040117

Bruun, P., 1954. Coast Erosion and the Development of Beach Profiles, US Army Corps of Engineers, 44. US Beach Erosion Board.

Cáceres, I., Sánchez-Arcilla, A., Zanuttigh, B., Lamberti, A., Franco, L., 2005. Wave overtopping and induced currents at emergent low crested structures. Coast. Eng. 52 (10—11), 931—947. https://doi.org/10.1016/j.coastaleng.2005.09.004

Cáceres, I., Stive, M.J.F., Sánchez-Arcilla, A., Trung, L.H., 2008. Quantification of changes in current intensities induced by wave overtopping around low-crested structures. Coast. Eng. 55 (2), 113—124. https://doi.org/10.1016/j.coastaleng.2007.09.003

Charlier, R.H., de Meyer, C.P., 1989. Coastal defense and beach renovation. Ocean and Shoreline Management 12 (5—6), 525—543. https://doi.org/10.1016/0951-8312(89)90029-5

Chen, Q., 2006. Fully Nonlinear Boussinesq-Type Equations for Waves and Currents over Porous Beds. J. Eng. Mech. 132 (2), 220—230. https://doi.org/10.1061/(asce)0733-9399(2006)132:2(220)

Chen, Q., Dalrymple, R.A., Kirby, J.T., Kennedy, A.B., Haller, M.C., 1999. Boussinesq modeling of a rip current system. J. Geophys. Res. Oceans 104 (C9), 20617—20637. https://doi.org/10.1029/1999jc900154

Chen, Q., Kirby, J.T., Dalrymple, R.A., Shi, F., Thornton, E.B., 2003. Boussinesq modeling of longshore currents. J. Geophys. Res. Oceans 108 (C11). https://doi.org/10.1029/2002jc001308

Christou, M., Swan, C., Gudmestad, O.T., 2008. The interaction of surface water waves with submerged breakwaters. Coast. Eng. 55 (12), 945—958. https://doi.org/10.1016/j.coastaleng.2008.02.014

Dean, R., G., 1977. Equilibrium beach profiles: US Atlantic and Gulf coasts. Department of Civil Engineering and College of Marine Studies., University of Delaware.

Deltares Delft Hydraulics, 1997. Two-dimensional and one-dimensional model simulations for the effect of a single detached breakwater on the shore. Deltares (WL), Delft, Netherlands.

Dette, H.H., Larson, M., Murphy, J., Newe, J., Peters, K., Reniers, A., Steetzel, H., 2002. Application of prototype flume tests for beach nourishment assessment. Coast. Eng. 47 (2), 137—177. https://doi.org/10.1016/S0378-3839(02)00124-2

Divinsky, B.V., Kosyan, R.D., 2020. Influence of the climatic variations in the wind waves parameters on the alongshore sediment transport. Oceanologia 62 (2), 190—199. https://doi.org/10.1016/j.oceano.2019.11.002

Divinsky, B.V., Ryabchuk, D.V., Kosyan, R.D., Sergeev, A.Y., 2021. Development of the sandy coast: Hydrodynamic and morphodynamic conditions (on the example of the Eastern Gulf of Finland). Oceanologia 63 (2), 214—226. https://doi.org/10.1016/j.oceano.2020.12.002

Ding, Y., Wang, S.S.Y., 2008. Development and Application of a Coastal and Estuarine Morphological Process Modeling System. J. Coastal Res. 10052, 127—140. https://doi.org/10.2112/1551-5036-52.sp1.127

Do, J.D., Jin, J.Y., Hyun, S.K., Jeong, W.M., Chang, Y.S., 2020. Numerical investigation of the effect of wave diffraction on beach erosion/accretion at the Gangneung Harbor. Korea. J. Hydro-Environ. Res. 29, 31—44. https://doi.org/10.1016/j.jher.2019.11.003

Feddersen, F., Clark, D.B., Guza, R.T., 2011. Modeling surf zone tracer plumes: 1. Waves, mean currents, and low-frequency eddies. J. Geophys. Res. Oceans, 116(C11). https://doi.org/10.1029/2011JC007210

French, P., 2001. Coastal Defences Processes, Problems and Solution. Taylor & Francis Group. https://doi.org/10.4324/9780203187630

Galappatti, G., Vreugdenhil, C.B., 1985. A depth-integrated model for suspended sediment transport. J. Hydraulic Res. 23. https://doi.org/10.1080/00221688509499345

Galappatti, R., 1983. A depth integrated model for suspended transport. Communications on Hydrology - Delft University of Technology, Department of Civil Engineering Report, 83—7.

Gallerano, F., Cannata, G., Lasaponara, F., 2016. A new numerical model for simulations of wave transformation, breaking and long-shore currents in complex coastal regions. Int. J. Numer. Methods Fluids. 80 (10), 571—613. https://doi.org/10.1002/fld.4164

Geiman, J.D., Kirby, J.T., Reniers, A.J.H.M., MacMahan, J.H., 2011. Effects of wave averaging on estimates of fluid mixing in the surf zone. J. Geophys. Res. Oceans 116 (C4). https://doi.org/10.1029/2010JC006678

Gorrick, S., Rodríguez, J.F., 2014. Scaling of sediment dynamics in a laboratory model of a sand-bed stream. J. Hydro-Environ 8 (2), 77—87. https://doi.org/10.1016/j.jher.2013.12.001.

Grasmeijer, B., 2002. Process-Based Cross-Shore Modeling of Barred Beaches Ph.D. Thesis. Utrecht University, Utrecht, The Netherlands.

Hieu, P.D., Phan, V.N., Nguyen, V.T., Nguyen, T.V., Tanaka, H., 2020. Numerical study of nearshore hydrodynamics and morphology changes behind offshore breakwaters under actions of waves using a sediment transport model coupled with the SWASH model. Coast. Eng. J. 62 (4), 553—565. https://doi.org/10.1080/21664250.2020.1828016

Holthuijsen, L.H., Herman, A., Booij, N., 2003. Phase-decoupled refraction-diffraction for spectral wave models. Coast. Eng. 49 (4), 291—305. https://doi.org/10.1016/S0378-3839(03)00065-6

Isobe, M., Horikawa, K., 1982. Study on water particle velocities of shoaling and breaking waves. Coast. Eng. 25 (1), 109—123. https://doi.org/10.1080/05785634.1982.11924340

Johnson, D., Pattiaratchi, C., 2006. Boussinesq modelling of transient rip currents. Coast. Eng. 53 (5—6), 419—439. https://doi.org/10.1016/j.coastaleng.2005.11.005

Karambas, T.V., 2012. Design of detached breakwaters for coastal protection: development and application of an advanced numerical model. Coast. Eng. Proc. 1—6. https://doi.org/10.9753/icce.v33.sediment.115

Karambas, T.V., Koutitas, C., 2002. Surf and Swash Zone Morphology Evolution Induced by Nonlinear Waves. J. Waterw. Port Coast. Ocean Eng. 128 (3), 102—113. https://doi.org/10.1061/(asce)0733-950x(2002)128:3(102)

Karambas, T.V., Samaras, A.G., 2017. An integrated numerical model for the design of coastal protection structures. J. Mar. Sci. Eng. 5 (4), 50. https://doi.org/10.3390/jmse5040050

Katopodi, I., Ribberink, J.S., 1992. Quasi-3D modelling of suspended sediment transport by currents and waves. Coast. Eng. 18 (1—2), 83—110. https://doi.org/10.1016/0378-3839(92)90006-G

Kennedy, A.B., Kirby, J.T., Chen, Q., Dalrymple, R.A., 2001. Boussinesq-type equations with improved nonlinear performance. Wave Motion 33 (3), 225—243. https://doi.org/10.1016/S0165-2125(00)00071-8

Klonaris, G.T., Memos, C.D., Drønen, N.K., 2016. High-Order Boussinesq-Type Model for Integrated Nearshore Dynamics. J. Waterw. Port Coast. Ocean Eng. 142 (6), 04016010. https://doi.org/10.1061/(asce)ww.1943-5460.0000349

Klonaris, G.T., 2016. Morphodynamics in a beach with submerged breakwaters. NTUA Athens, Greece.

Klonaris, G.T., Memos, C.D., Drønen, N.K., Deigaard, R., 2018. Simulating 2DH coastal morphodynamics with a Boussinesq-type model. Coast. Eng. J. 60 (2), 159—179. https://doi.org/10.1080/21664250.2018.1462300

Klonaris, G.T., Metallinos, A.S., Memos, C.D., Galani, K.A., 2020. Experimental and numerical investigation of bed morphology in the lee of porous submerged breakwaters. Coast. Eng. 155, 103591. https://doi.org/10.1016/j.coastaleng.2019.103591

Kobayashi, H., Watanabe, A., Isobe, M., Sato, S., Ishii, T., 2000. Three-dimensional beach deformation model for nonlinear multi-directional waves. In: 2000 — Proceedings of the 27th International Conference on Coastal Engineering. ICCE 2000 https://doi.org/10.1061/40549(276)213

Kobayashi, N., 2016. Coastal Sediment Transport Modeling for Engineering Applications. J. Waterw. Port Coast. Ocean Eng. 142 (6), 03116001. https://doi.org/10.1061/(asce)ww.1943-5460.0000347

Kristensen, S.E., Drønen, N., Deigaard, R., Fredsoe, J., 2016. Impact of groyne fields on the littoral drift: A hybrid morphological modelling study. Coast. Eng. 111, 13—22. https://doi.org/10.1016/j.coastaleng.2016.01.009

Larsen, J., Dancy, H., 1983. Open boundaries in short wave simulations - A new approach. Coast. Eng. 7 (3), 285—297. https://doi.org/10.1016/0378-3839(83)90022-4

Larson, M., Kubota, S., Erikson, L., 2004. Swash-zone sediment transport and foreshore evolution: Field experiments and mathematical modeling. Mar. Geol. 212 (1—4), 61—79. https://doi.org/10.1016/j.margeo.2004.08.004

Larson, M., Wamsley, T.V., 2007. A formula for longshore sediment transport in the Swash. In: Coastal Sediments '07 — Proceedings of 6th International Symposium on Coastal Engeneering and Science of Coastal Sediment Processes. https://doi.org/10.1061/40926(239)151

Leont'yev, I.O., 1996. Numerical modelling of beach erosion during storm event. Coast. Eng. 29 (1—2), 187—200. https://doi.org/10.1016/S0378-3839(96)00029-4

Lesser, G.R., Roelvink, J.A., van Kester, J.A.T.M., Stelling, G.S., 2004. Development and validation of a three-dimensional morphological model. Coast. Eng. 51 (8—9), 883—915. https://doi.org/10.1016/j.coastaleng.2004.07.014

Malej, M., Shi, F., Smith, J. M., 2019. Modeling ship-wake-induced sediment transport and morphological change—sediment module in FUNWAVE-TVD. Technical Note (Engineer Research and Development Center (U.S.)). https://doi.org/10.21079/11681/32911

Madsen, P.A., Sørensen, O.R., Schäffer, H.A., 1997. Surf zone dynamics simulated by a Boussinesq type model. Part I. Model description and cross-shore motion of regular waves. Coast. Eng. 32 (4), 255287. https://doi.org/10.1016/S0378-3839(97)00028-8

Mahmoudof, S.M., Hajivalie, F., 2021. Experimental study of hydraulic response of smooth submerged breakwaters to irregular waves. Oceanologia 63 (4), 448—462. https://doi.org/10.1016/j.oceano.2021.05.002

Masselink, G., Russell, P., Turner, I., Blenkinsopp, C., 2009. Net sediment transport and morphological change in the swash zone of a high-energy sandy beach from swash event to tidal cycle time scales. Mar. Geol. 267 (1—2), 18—35. https://doi.org/10.1016/j.margeo.2009.09.003

Ming, D., Chiew, Y.-M., 2000. Shoreline Changes behind Detached Breakwater. J. Waterw. Port Coast. Ocean Eng. 126 (2), 63—70. https://doi.org/10.1061/(asce)0733-950x(2000)126:2(63)

Nwogu, O., Takayama, T., Ikeda, N., 1992. Living with shore protection structures: A review. Report of Port and Harbour Research Institute 31 (2), 3—19.

Nam, P.T., Larson, M., Hanson, H., 2011. A numerical model of beach morphological evolution due to waves and currents in the vicinity of coastal structures. Coast. Eng. 58 (9), 863—876. https://doi.org/10.1016/j.coastaleng.2011.05.006

Nam, P.T., Larson, M., Hanson, H., Hoan, L.X., 2009. A numerical model of nearshore waves, currents, and sediment transport. Coast. Eng. 56 (11—12), 1084—1096. https://doi.org/10.1016/j.coastaleng.2009.06.007

Nordstrom, K.F., 2014. Living with shore protection structures: A review. Estuar. Coast. Shelf Sci. 50, 11—23. https://doi.org/10.1016/j.ecss.2013.11.003

Postacchini, M., Russo, A., Carniel, S., Brocchini, M., 2016. Assessing the Hydro-Morphodynamic Response of a Beach Protected by Detached, Impermeable, Submerged Breakwaters: A Numerical Approach. J. Coastal Res. 32 (3), 590—602. https://doi.org/10.2112/JCOASTRES-D-15-00057.1

Pranzini, E., Wetzel, L., Williams, A.T., 2015. Aspects of coastal erosion and protection in Europe. J. Coast. Conserv. 19. https://doi.org/10.1007/s11852-015-0399-3

Ranasinghe, R., Larson, M., Savioli, J., 2010. Shoreline response to a single shore-parallel submerged breakwater. Coast. Eng. 57 (11—12), 1006—1017. https://doi.org/10.1016/j.coastaleng.2010.06.002

Razak, M.S.A., Nor, N.A.Z.M., 2018. XBeach Process-Based Modelling of Coastal Morphological Features Near Breakwater. MATEC Web of Conferences. https://doi.org/10.1051/matecconf/201820301007

Ribberink, J.S., 1998. Bed-load transport for steady flows and unsteady oscillatory flows. Coast. Eng. 34 (1—2), 59—82. https://doi.org/10.1016/S0378-3839(98)00013-1

Roelvink, D., Costas, S., 2019. Coupling nearshore and aeolian processes: XBeach and duna process-based models. Environ. Model Softw. 115, 98—112. https://doi.org/10.1016/j.envsoft.2019.02.010

Ruiz-Martínez, G., Mariño-Tapia, I., Baldwin, E.G.M., Casarín, R.S., Ortiz, C.E.E., 2016. Identifying Coastal Defence Schemes through Morphodynamic Numerical Simulations along the Northern Coast of Yucatan. Mexico. J. Coastal Res. 32 (3), 651—669. https://doi.org/10.2112/JCOASTRES-D-15-00009.1

Seabergh, W.C., Kraus, N.C., 2003. Progress in management of sediment bypassing at coastal inlets: Natural bypassing, weir jetties, jetty spurs, and engineering aids in design. Coast. Eng. J. 45 (04), 533—563. https://doi.org/10.1142/S0578563403000944

Servold, K.P., Webb, B.M., Douglass, S.L., 2017. Effects of Low-Crested Living Shoreline Breakwaters on Wave Setup, in: Coastal Structures and Solutions to Coastal Disasters 2015: Resilient Coastal Communities - Proceedings of the Coastal Structures and Solutions to Coastal Disasters Joint Conference 2015. https://doi.org/10.1061/9780784480304.045

Shi, F., Kirby, J.T., Harris, J.C., Geiman, J.D., Grilli, S.T., 2012. A high-order adaptive time-stepping TVD solver for Boussinesq modeling of breaking waves and coastal inundation. Ocean Model. 43, 36—51. https://doi.org/10.1016/j.ocemod.2011.12.004

Smagorinsky, J., 1963. General circulation experiments wiht the primitive equations I. The basic experiment. Mon. Weather Rev. 91.

Smit, P.B., Janssen, T.T., Herbers, T.H.C., 2015. Stochastic modeling of inhomogeneous ocean waves. Ocean Model. 96, 26—35. https://doi.org/10.1016/j.ocemod.2015.06.009

Tang, J., Lyu, Y., Shen, Y., Zhang, M., Su, M., 2017. Numerical study on influences of breakwater layout on coastal waves, wave-induced currents, sediment transport and beach morphological evolution. Ocean Eng. 141, 375—387. https://doi.org/10.1016/j.oceaneng.2017.06.042

Tonelli, M., Petti, M., 2009. Hybrid finite volume - finite difference scheme for 2DH improved Boussinesq equations. Coast. Eng. 56 (5—6), 609—620. https://doi.org/10.1016/j.coastaleng.2009.01.001

Tsiaras, A.-C., Karambas, T., Koutsouvela, D., 2020. Design of Detached Emerged and Submerged Breakwaters for Coastal Protection: Development and Application of an Advanced Numerical Model. J. Waterw. Port Coast. Ocean Eng. 146 (4), 04020012. https://doi.org/10.1061/(asce)ww.1943-5460.0000566

Valsamidis, A., Reeve, D.E., 2017. Modelling shoreline evolution in the vicinity of a groyne and a river. Cont. Shelf Res. 132, 49—57. https://doi.org/10.1016/j.csr.2016.11.010

van Rijn, L., 1993. In: Principles of Sediment Transport in Rivers, Estuaries and Coastal Seas, 1006. Aqua publications, Amsterdam, 11—13.

van Rijn, L.C., 2011. Coastal erosion and control. Ocean and Coastal Manag. 54 (12), 867—887. https://doi.org/10.1016/j.ocecoaman.2011.05.004

van Rijn, L., C., 2013. Design of hard coastal structures against erosion. Accessed online: https://www.leovanrijn-sediment.com/papers/Coastalstructures2013.pdf.

Watanabe, A., 1988. In: Horikawa, K. (Ed.), University of Tokyo Press, Tokyo.

Wei, G., Kirby, J.T., Sinha, A., 1999. Generation of waves in Boussinesq models using a source function method. Coast. Eng. 36 (4), 271—299. https://doi.org/10.1016/S0378-3839(99)00009-5

Zyserman, J.A., Johnson, H.K., 2002. Modelling morphological processes in the vicinity of shore-parallel breakwaters. Coast. Eng. 45 (3—4), 261—284. https://doi.org/10.1016/S0378-3839(02)00037-6